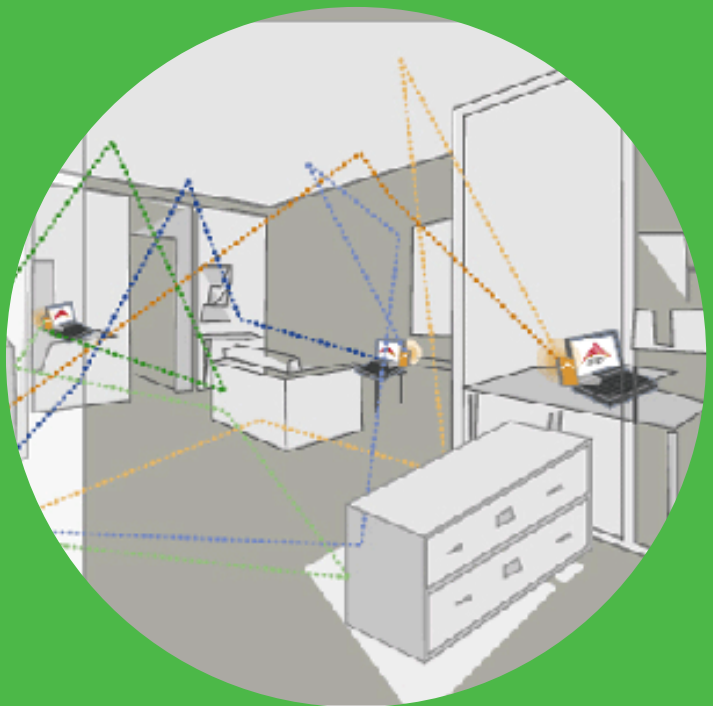


Millimeter Wave and UWB Propagation for High Throughput Indoor Communications

Suiyan Geng



Millimeter Wave and UWB Propagation for High Throughput Indoor Communications

Suiyan Geng

Doctoral dissertation for the degree of Doctor of Science in Technology to be presented with due permission of the School of Electrical Engineering for public examination and debate in Auditorium S3 at the Aalto University School of Electrical Engineering (Espoo, Finland) on the 2nd of November 2011 at 12 noon.

**Aalto University
School of Electrical Engineering
Department of Radio Science and Engineering
Radio Engineering**

Supervisor

Professor Pertti Vainikainen

Instructor

Professor Pertti Vainikainen

Preliminary examiners

Doctor Chia-Chin Chong

Professor Hirokazu Sawada

Opponent

Professor Fredrik Tufvesson

Aalto University publication series

DOCTORAL DISSERTATIONS 97/2011

© Suiyan Geng

ISBN 978-952-60-4318-0 (pdf)

ISBN 978-952-60-4317-3 (printed)

ISSN-L 1799-4934

ISSN 1799-4942 (pdf)

ISSN 1799-4934 (printed)

Unigrafia Oy

Helsinki 2011

Finland

The dissertation can be read at <http://lib.tkk.fi/Diss/>

Publication orders (printed book):

julkaisut@aalto.fi

Author

Suiyan Geng

Name of the doctoral dissertation

Millimeter Wave and UWB Propagation for High Throughput Indoor Communications

Publisher School of Electrical Engineering

Unit Department of Radio Science and Engineering

Series Aalto University publication series DOCTORAL DISSERTATIONS 97/2011

Field of research Radio Engineering

Manuscript submitted 15 June 2010

Manuscript revised 26 September 2011

Date of the defence 2 November 2011

Language English

Monograph

Article dissertation (summary + original articles)

Abstract

Millimeter-wave systems at 60 GHz and ultra-wideband (UWB) systems in the microwave range of 3-10 GHz have been received with great interest for their high data rate wireless communications. In design, test and optimization of future wireless systems, channel models featuring the relevant characteristics of radiowave propagation are required. Furthermore, detailed understanding of the propagation channel and its interaction with system, creates insights into possible solutions.

In this work, both theoretical (ray-tracing) and statistical models of the 60 GHz and UWB channels are studied. Propagation characteristics of the 60 GHz and UWB indoor channels are also compared for providing useful information on design of radio systems. More specifically, based on real-time channel sounder measurements performed in the 60 GHz band, propagation mechanisms including person blocking effect are concluded. Ray-based models in LOS and NLOS indoor corridors are proposed. Multipath power distributions in the 60 GHz band are studied first time. Moreover, propagation interdependencies of path loss, shadowing, number of paths, Rice K-factor and cross polarization discrimination (XPD) with channel delay spread are established. In the UWB propagation channel, frequency- and bandwidth-dependencies are investigated. Multipath and clustering propagation characteristics are analyzed. A new cluster model is proposed and compared with the classical Saleh-Valenzuela model for gaining more understanding of channel general properties. Finally, the performance and capacities of the 60 GHz UWB and MIMO (multiple-in and multiple-out) systems are analyzed for providing reliable parameters for system design and useful information for standardization groups.

Keywords Millimeter-waves, ultra-wideband (UWB), propagation, ray-based models, statistical models, multipath, clustering, multiple-in and multiple-out (MIMO).

ISBN (printed) 978-952-60-4317-3

ISBN (pdf) 978-952-60-4318-0

ISSN-L 1799-4934

ISSN (printed) 1799-4934

ISSN (pdf) 1799-4942

Location of publisher Espoo

Location of printing Helsinki

Year 2011

Pages 115

The dissertation can be read at <http://lib.tkk.fi/Diss/>

PREFACE

This thesis was carried out at the Department of Radio Science and Engineering of Aalto University (Helsinki University of Technology previously). Thanks for Nokia Foundation for the financial support for the work.

I'm grateful to my supervisor, Professor Pertti Vainikainen, for the opportunity to work for several research projects associated with radiowave propagation. Thanks for his support, help and guidance throughout the whole course of the work.

I would also like to thank Professor Antti Räisänen for his help during the period of my study in the department. Thanks to Dr. Jarmo Kivinen for his measurement experience in the 60 GHz channel sounding measurements. Thanks also to Stina Lindberg, Viktor Sibakov and Lorenz Schmuckli for their assistance and help. All my colleagues at the Department of Radio Science and Engineering deserve my thanks for their assistance and for contributing towards a scientific work environment.

Finally, I would like to express my heartiest thanks to my husband Xiongwen Zhao, for his continuous support and deep understanding, to my elder daughter Jing for her excellent school scores that make me proud, and to my little daughter Yuan for her smiles and telling day-care stories. Thank you all for your patience and support!

Helsinki, April 2010.

Suiyan Geng

TABLE OF CONTENTS

ABSTRACT	3
PREFACE	5
TABLE OF CONTENTS	6
LIST OF PUBLICATIONS	8
LIST OF SYMBOLS	9
1. INTRODUCTION	11
1.1 Background.....	11
1.2 Objectives and contents of the thesis.....	11
1.3 New scientific results.....	12
2. PROPAGATION CHANNEL CHARACTERIZATION.....	13
2.1 Introduction.....	13
2.2 Channel fading.....	13
2.2.1 Large-scale fading.....	14
2.2.2 Small-scale fading.....	15
2.3 Ray-based models.....	16
2.3.1 Reflection.....	16
2.3.2 Diffraction.....	16
2.3.2.1 <i>Uniform theory of diffraction</i>	16
2.3.2.2 <i>Heuristic diffraction coefficients</i>	17
2.4 Statistical modelling.....	18
2.4.1 Statistical parameters	19
2.4.1.1 <i>Number of paths</i>	19
2.4.1.2 <i>Delay spread</i>	19
2.4.1.3 <i>Cross polarization discrimination</i>	20
2.4.2 Statistical models	20
2.4.2.1 <i>Average power delay profile</i>	20
2.4.2.2 <i>Saleh-Valenzuela cluster model</i>	20
2.5 UWB and 60 GHz channel measurements and data analysis	21
2.5.1 UWB measurement setup and environments.....	22
2.5.2 The 60 GHz propagation measurements.....	22
3. ULTRAWIDE-BAND (UWB) RADIOS IN THE MICROWAVE RANGE (3-10 GHz).....	23
3.1 Introduction.....	23
3.2 Clustering channel characterization.....	23
3.2.1 Single-cluster channel.....	23
3.2.1.1 <i>Single-exponential power delay profile</i>	23
3.2.1.2 <i>Forms of multipath components</i>	23
3.2.2 Multi-cluster channel.....	24
3.2.2.1 <i>Multi-cluster specification</i>	24
3.2.2.2 <i>A modified multi-cluster model</i>	25
3.3 Frequency dependence of UWB channel.....	27

3.4 Bandwidth dependence of UWB channel.....	28
3.5 Fading robustness of UWB signals.....	29
3.6 Findings about UWB propagation channels in this work.....	29
4. MILLIMETER-WAVE (60 GHZ) BAND.....	30
4.1 Introduction.....	30
4.2 Mm-wave propagation mechanisms.....	30
4.3 Ray-based models in indoor corridors.....	30
4.3.1 LOS corridor.....	31
4.3.2 NLOS corridor.....	32
4.4 Multipath power distributions.....	32
4.4.1 Distributions in mobile radio channels	33
4.4.2 Rayleigh and double-Rayleigh distributions	33
4.4.3 Multiple-Rayleigh distribution.....	34
4.5 Interdependence of channel characteristics.....	34
4.6 Characteristics of mm-wave propagation signals.....	35
4.7 Findings about 60 GHz propagation channels in this work.....	36
5. PERFORMANCE AND CAPACITY ANALYSIS OF 60 GHZ UWB AND MIMO SYSTEMS.....	37
5.1 Introduction.....	37
5.2 Channel capacities.....	37
5.3 Radio link budgets	37
5.4 The 60 GHz UWB system performance analysis.....	38
5.5 The 60 GHz MIMO system capacity analysis.....	39
6. SUMMARY OF PUBLICATIONS	41
7. CONCLUSIONS	43
REFERENCES	44

LIST OF PUBLICATIONS

- [P1] **S. Geng**, J. Kivinen, X. Zhao and P. Vainikainen, "Millimeter-wave propagation channel characterization for short-range wireless communications," *IEEE Transactions on Vehicular Technology*, vol. 58, no. 1, pp. 3-13, Jan. 2009.
- [P2] **S. Geng** and P. Vainikainen, "Millimeter-wave indoor channel characterization for broadband wireless local area networks," *the IASTED International Conference on Antenna, Radar, and Wave Propagation (ARP'07)*, Montreal, Canada, May 30- June 1, 2007, pp. 170-175.
- [P3] **S. Geng** and P. Vainikainen, "Mm-wave propagation in indoor corridors," *IEEE Antennas and Wireless Propagation Letters (AWPL)*, vol. 8, pp. 1242-1245, 2009.
- [P4] **S. Geng**, S. Ranvier, X. Zhao, J. Kivinen, and P. Vainikainen, "Multipath propagation characterization of ultra-wide band indoor radio channels," *2005 IEEE International Conference on Ultra-Wideband (ICUWB05)*, Zurich, Switzerland, Sep. 5-8, 2005, pp. 11-15.
- [P5] **S. Geng** and P. Vainikainen, "Clustering characterization for UWB indoor communications," *IEEE European Conference on Antennas and Propagation (EuCAP)*, Barcelona, Spain, April 12-16, 2010, papMo-83.pdf.
- [P6] **S. Geng** and P. Vainikainen, "Frequency and bandwidth dependency of UWB propagation channels," *IEEE International Symposium on Personal, Indoor and Mobile Radio Communications (PIMRC06)*, Helsinki, Finland, Sep. 11-14, 2006, CD-ROM (1-4244-0330-8), papTH6_1.pdf.
- [P7] **S. Geng** and P. Vainikainen, "Experimental Investigation of the Properties of Multiband UWB Propagation Channels," *IEEE International Symposium on Personal, Indoor and Mobile Radio Communications (PIMRC07)*, Athens, Greek, Sept. 3-7, 2007, CD-ROM (1-4244-01144-0), pap337.pdf.
- [P8] **S. Geng**, "Performance and capacity analysis of 60 GHz WPAN channel," *Microwave and Optical Technology Letters*, vol. 51, no. 11, pp. 2671-2675, Nov. 2009.

The author of this thesis completed the numerical calculations and prepared the manuscript in [P1-P8]. In [P1][P4], Dr. Jarmo Kivinen and Dr. Sylvain Ranvier had the main responsibilities for the 60 GHz [P1] and UWB [P4] measurement setups, respectively. All publications were supervised by Prof. Pertti Vainikainen, who should also appear as the co-author in [P8] but does not, as the paper was published without any revision.

LIST OF SYMBOLS

B	Bandwidth
BE	Blocking effect
c_0	Speed of light in free space
C_{MIMO}	Capacity for MIMO channel
C_{SISO}	Capacity for SISO channel
d_L	Distance along a LOS route
d_{NL}	Distance along a NLOS route
D_H	Holm's diffraction coefficient
D_L	Luebbers' diffraction coefficient
D_{TE}	Electric wave vector with perpendicular incidence to the edge of wedge
D_{TM}	Electric wave vector with parallel incidence to the edge of wedge
E_{UTD}	Electric field of uniform theory of diffraction
$F(d)$	Large-scale fading
FM	Fading margin
$F(x)$	Transition function
G_r	Antenna gain at receiver
G_t	Antenna gain at transmitter
$h(\cdot)$	Impulse response
H	Multiple Rayleigh fading signal
HH^+	Normalized channel matrix H with transpose-conjugate
IL	Implementation loss
K	Rice K-factor
$K_0(\cdot)$	Modified Bessel function of the second kind and zero order
K_l	Number of rays within lth cluster
L	Number of clusters
MB	Multiband
n	Path loss exponent
N	Number of multipaths
N_0	Noise power
NF	Noise figure
N_R	Number of receiver antenna
N_T	Number of transmitter antenna
$p(\gamma)$	Probability density function of variable γ
$p(T_l T_{l-1})$	Poisson process of clusters with arrival time T
$p(\tau_{kl} \tau_{k-1,l})$	Poisson process of rays with arrival time τ
$p_z(z)$	Probability density function of double-Rayleigh distribution of variable z
PBE	Person blocking effect
\overline{PL}	Mean path loss

PL_0	Free space path loss
P_r	Received power
P_t	Transmitted power
$P(\gamma)$	Cumulative density function of variable γ
$P(\tau)$	Power decay function
$P(\phi)$	Power angle profile
$Q(\cdot)$	Standard cumulative error function of normal distribution
R	Fresnel reflection coefficient
SB	Single-band
SNR	Signal to noise ratio
S_σ	Shadow fading with standard deviation of σ
XPD	Cross polarization discrimination
X_σ	Gaussian Random variable with zero mean and standard deviation of σ
α	Power decay rate
β_{kl}	Signal amplitude for kth ray within the lth cluster
$\overline{\beta^2(0,0)}$	Average power of the first arrival ray of the first cluster
γ	Ray decay rate
Γ	Cluster decay rate
$\delta(\cdot)$	Delta function
ε_r	Relative complex permittivity
θ	Angle in elevation
λ	Ray arrival rate
λ_0	Wavelength in free space
Λ	Cluster arrival rate
σ_τ	Rms delay spread
τ	Delay
$\bar{\tau}$	Mean excess delay
ϕ	Angle in azimuth

1. INTRODUCTION

1.1. Background

Today, in many countries, most of the available spectrum has been allocated. This results in scarcity of the radio spectrum, which poses a serious problem for the development of future wireless communications systems. Moreover, the current wireless systems are incapable to offer gigabit transmission due to their small bandwidths and their subsequently low capacity. Meanwhile, applications with high data rate up to several gigabit WPAN (wireless personal area network) applications are emerging. These applications can be wireless A/V (audio/video) cable replacements, wireless high speed file transfer applications capable of downloading hour-long movie files within one minute, etc. Currently, there are two major radio candidates enabling wireless interface for such high-rate applications, namely, UWB (ultra-wideband) radios in microwave range 3.1-10.6 GHz and in millimeter-wave 60 GHz band.

The specified UWB spectrum and 60 GHz band have been proposed for short-range (<10 m) WPAN applications, with data rates of 110- 480 Mbps and >1 Gbps, respectively, conforming to the IEEE 802.15.3a and IEEE 802.15.3c standards [1]-[4]. In order to effectively employ the UWB and 60 GHz radio systems, channel models featuring the relevant characteristics are required. Moreover, the design, testing, and improvement of wireless systems hinge critically on our understanding of the propagation channel. Understanding of the propagation channel and its interaction with system, can create insights into solutions. One of the key goals of this work is to increase our knowledge about the interaction between channel characteristics and UWB and 60 GHz radio systems. In addition to publications [P1-P8] of this work, the UWB and mm-wave propagation channel measurements and modeling are also presented in [5]-[11].

The indoor propagation channel is complicated and diverse, as different structures cause different propagation phenomena, i.e., reflection, refraction, diffraction and scattering which result in multipath propagation. Modeling the multipath propagation channel is typically done in a theoretical (ray-tracing) or statistical fashion based on propagation channel measurements. Statistical models and parameters are useful in describing channel general properties which are required in system design. Ray-based models are based on exact computations which make use of the information of the physical processes and reliably generated data in characterizing the main features of a propagation channel.

1.2. Objectives and contents of the thesis

Characterization of a propagation channel depends largely on measurement systems. For example, polarization (vertical and/or horizontal) measurements are necessarily required in ray-based models for comparing the proposed model with measurement data in order to validate the accuracy of the model. The 60 GHz channel measurements were performed in time-domain by using real-time channel sounder for direction-of-arrival (DOA) and continuous-route (CR) measurement campaigns. Therefore, more comprehensive studies on 60 GHz propagation including large scale and small scale characteristics [P1][P2][P3], statistical

models [P1][P2] and ray-based models [P3] are presented and introduced in Chapter 2. Moreover, propagation characteristics in 60 GHz and UWB indoor channels are compared in [P4] to gain more understanding of the channels' general properties.

In Chapter 3, UWB channel multipath and clustering characteristics are investigated [P4]. A new cluster model is proposed [P5] and compared with the conventional Saleh-Valenzuela model (which is proposed in IEEE 802.15.3a and 4a for UWB systems) for providing useful information for standardization groups. Moreover, frequency- and bandwidth- dependencies of UWB propagation channels are inspected [P6][P7]. The main features of the UWB radio are specified to pave the path for analyzing the 60 GHz UWB system later in [P8].

In Chapter 4, studies of the 60 GHz channel also focus on propagation mechanisms [P1], multipath power distributions [P3], and propagation interdependencies of path loss, shadowing, number of paths, Rice K -factor and cross polarization discrimination (XPD) with channel delay spread [P1][P2]. Finally, the unique characteristics of mm-wave propagation signals are pointed out. To provide reliable parameters for system design and useful information for standardization groups, the performance and capacities of the 60 GHz UWB and MIMO (multiple-in and multiple-out) systems [P8] are analyzed in Chapter 5.

1.3. New scientific results

The thesis contains the following new scientific results:

- 1) Mm-wave 60 GHz band propagation mechanisms, including person block effect, are established [P1][P8].
- 2) Interdependencies of different propagation characteristics on channel delay spread (DS) are established [P1][P2].
- 3) Ray-based models in LOS and NLOS indoor corridors are proposed [P3].
- 4) Multipath power distributions in indoor corridors in 60 GHz band are studied first time [P3].
- 5) UWB (3-10 GHz) and 60 GHz propagation characteristics are compared [P4][P8].
- 6) New cluster models for UWB channels are proposed [P5].
- 7) Frequency and bandwidth dependencies of UWB channel propagation characteristics are investigated [P6][P7].
- 8) Radio link budgets, including path loss and shadow fading models for high throughput 60 GHz UWB and MIMO systems, are provided [P8].

2. PROPAGATION CHANNEL CHARACTERIZATION

2.1 Introduction

Indoor wireless communications have generated a huge interest in recent years. There are more and more users gathering in crowded spaces like airports, hotels, conference halls, class rooms, and other venues where the applications are likely to include wireless access to local area networks (LANs), the successful implementation of which is determined by the propagation channel in which the system operates. A detailed understanding of channel and its interaction with systems is likely to create insights into possible solutions. Therefore, in this work, the UWB (3-10 GHz) and 60 GHz propagation channel characteristics are analyzed and compared to gain more understanding into general channel properties and their implications with systems.

The indoor propagation channel is a complicated and diverse entity, as different structures cause various propagation phenomena such as reflection, refraction, diffraction and scattering which result in multipath propagation. Modeling the multipath propagation channel is typically done in a theoretical (ray-tracing) or statistical fashion. Since channel fading degrades the system's performance, it is of major concern for propagation research and system deployment.

2.2 Channel fading

Fading is generally divided into large scale and small scale fading. Large scale fading is often characterized by mean path loss \overline{PL} and shadowing. \overline{PL} denotes the mean signal power loss and obeys the power distance law. Due to variations in the propagation environments, the signal power observed at a local area will deviate from its mean. This phenomenon is called shadowing or large scale fading, as illustrated in Fig. 2-1 [12]. Small scale fading describes the rapid fluctuations of the received signal strength over short travel distances or short time duration. However, the exact range over which the assumption is valid remains unknown. Typically, the local average power is computed by averaging the signal measurements over a range of 10λ to 40λ [12][13].

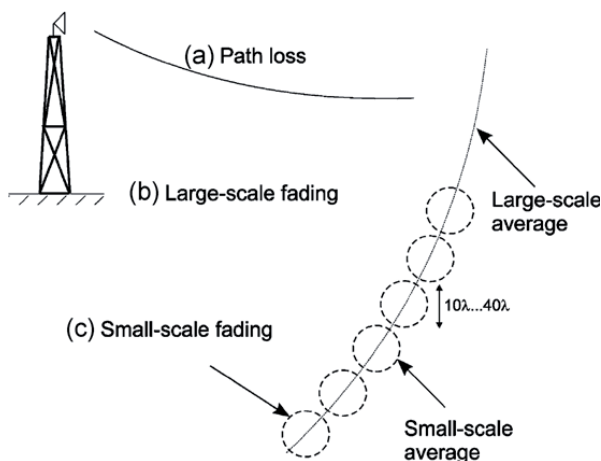


Fig. 2-1. Channel fading effects: path loss, shadowing (large scale fading) and small scale fading [12].

2.2.1 Large scale fading

Large scale fading of the channel $F(d)$ can be modeled as a combination of mean path loss $\overline{PL}(d)$ and shadowing and expressed as:

$$F(d) = \underbrace{PL_0(d_0) + 10n \log\left(\frac{d}{d_0}\right)}_{\text{mean path loss}} + \underbrace{S_\sigma}_{\text{shadowing}}, \quad (2-1)$$

where the free space path loss PL_0 at reference distance $d_0 = 1$ m (for indoor environments) is frequency-dependent, path loss exponent n is environment-dependent, and shadowing standard deviation (STD) σ is mainly system-dependent (e.g. narrow-band or UWB) [P4][P6]. Because of shadowing, a fading margin FM is often considered in link budget in wireless systems.

Studies [P1][P4][13] show that the mean values of PL exponent are in ranges of 1.6-1.8 and 3.0-3.2 for LOS and NLOS indoor environments, respectively. The fading margin $FM \approx 10$ dB for traditional narrow-band channels [P1][14], and is less than 4 dB with 90% link success probability for 500 MHz bandwidth UWB channels [P7]. Path loss and shadowing create key impacts on the *coverage* and *reliability* of radio systems [15]. Let's assume now that there is a coverage range predicted by the mean path loss with satisfactory (or 50% reliability), when a fading margin is considered, the system link success probability is increased greatly (typically 90%) at the fringe of coverage. Clearly, the stronger the signal variations due to fading, the larger the fading margin that has to be considered in the system design.

The mean path loss model $\overline{PL}(d)$ in Eq. (2-1) is obtained by using least square error fitting (LSEF) from the measurement data. However, the indoor propagation channel is quite complicated. This means that using the free space PL_0 at the reference distance d_0 is inaccurate in some cases (e.g., indoor corridors). Thus, the slope-intercept \overline{PL} model is employed in literature [16][17] is introduced by extracting the slope and intercept values directly from the measurement data:

$$\overline{PL}(d) = b + 10n \log_{10}(d), \quad (2-2)$$

where b is the intercept point and n is the slope in semi-log coordinates. The main advantage of the \overline{PL} model of Eq. (2-2) is that it avoids choosing the value of $PL_0(d_0)$. However, the model does not show the main feature of path loss which is frequency-dependent.

In this work, the \overline{PL} model of Eq. (2-1) is used in the 60 GHz propagation channel. Specifically, the free space path loss at the reference distance $d_0 = 1$ m is frequency-dependent, or $PL_0 = 68$ dB at 60 GHz. In the UWB channel, the difficulty being that the attenuation is not linear over the large bandwidth. In another words, using the wave length of the center frequency in \overline{PL} model of Eq. (2-1) is inaccurate. To avoid this, the slope-intercept \overline{PL} model of Eq. (2-2) is used in the UWB channel. It has been shown in many measurements that shadowing S_σ is well approximated by the log-normal distribution. In this work, shadowing is found to be normally distributed, when the power level is expressed in decibels for both narrow-band 60 GHz and UWB channels [P1][P7].

2.2.2 Small-scale fading

Multipath power distribution is important in evaluating the performance of various types of diversity, modulation and equalization techniques in wireless communications [13]. The Rayleigh and Rice distributions are commonly used to describe multipath distributions in NLOS and LOS environments. In LOS channel the Rice K -factor is important when defined as the power ratio between the LOS path and the mean of other multipath components:

$$K = A^2/2\sigma^2, \quad (2-3)$$

where A is the amplitude of the LOS path and σ indicates the standard deviation of either the real or the imaginary parts of the amplitude of multipath components.

It should be noted that the maximum likelihood method (ML) and the method of moment (MoM) are often used in the literature [18][19] to estimate the K -factor. In this work, both the ML and the MoM methods are used in extracting the K -factor for the 60 GHz channels [P2][P3].

Since there is no direct reference to the global statistics of multipaths, a lot of work is carried out to search for more accurate multipath distributions to fit with experimental data. Studies show that the Rayleigh, Rice [20], Nakagami [21], Suzuki [22] distributions fit well with the experimental measurement data for mobile radio channels at lower frequency bands. Recent studies show that double-Rayleigh [23] and multiple-Rayleigh [24] distributions agree well with measurement data and have a clear theoretical explanation.

It is well known that the magnitude of the complex Gaussian random variable is Rayleigh distributed. Furthermore, if there are two independent Rayleigh-distributed random variables denoted as x and y , the variable $z = xy$ will follow the double-Rayleigh distribution with probability density function (PDF) [23]:

$$p_z(z) = 2K_0(2\sqrt{z}), \quad (2-4)$$

where $K_0(\cdot)$ is the modified Bessel function of the second kind and zero order. Signals following the distribution of Eq. (2-4) are said to experience double- (or cascade) Rayleigh fading.

Similarly, higher order Rayleigh (e.g., triple Rayleigh) signals and their cumulative distribution functions (CDFs) can be generated. In [24], by assuming additive propagation processes, the multipath Rayleigh fading signal is expressed as:

$$H = K + H_1 + \alpha H_2 H_3 + \beta H_4 H_5 H_6 + \dots, \quad (2-5)$$

where K corresponds to a possible Rice factor, H_i follows the complex Gaussian or Rayleigh fading signal, the 3rd and 4th terms refer to the double-Rayleigh and triple-Rayleigh signals, and α and β are constants, which can be obtained by experimental data fitting.

In this work, the statistics of multipath powers in 60 GHz indoor are studied, but not for the UWB channel due to the measurement data being limited for statistical study. It is reported that for NLOS UWB channel with 7 GHz bandwidth fading statistics are no longer Rayleigh distributed but with the Ricean distribution [12].

2.3 Ray-based models

In design and optimization of future wireless systems, channel models featuring the relevant characteristics of radiowave propagation are required. Theoretical models are based on exact computations making use of information of the physical processes and reliable data of building in characterizing the main feature of a propagation channel. Ray tracing, using a high-frequency approximation of the Maxwell's equations, is a well-established tool for channel modelling. Specifically, ray tracing emits rays from the transmitter and computes the interaction of those rays with the environment. In the ray-tracing algorithm, reflection and diffraction are the main physical processes in LOS and NLOS environments. Moreover, the choice of reflection and diffraction coefficients is crucial in accurately predicting the signal power resulting from a physical process. Therefore, many researchers have studied and tried to modify the reflection [25]-[27] and diffraction coefficients [25][28]-[29] in ray-based models.

2.3.1 Reflection

Reflection occurs when a propagating electromagnetic wave is incident onto a boundary between two media with different material properties. The incident wave is partially reflected back into the first medium. It is well known that the Fresnel reflection coefficients are often used for predicting the specular reflection fields from smooth and infinity surfaces. The Fresnel reflection coefficient is expressed as a function of complex relative permittivity ϵ_r and angle of incidence θ_i for different polarization (i.e., vertical or horizontal) states [13].

2.3.2 Diffraction

Diffraction explains how radio wave can travel in an environment without the LOS path, i.e., when radio wave is obstructed by an impenetrable body. In indoor environments, a signal obstructed by a corner is quite usual. Therefore, various diffraction coefficients for right-angle lossy wedge (denoted as wedge hereafter unless specified) are studied in this work. Specifically, the uniform theory of diffraction (UTD) for perfectly conducting wedge, and heuristic diffraction coefficients for lossy wedges proposed by Luebbers and Holm are studied and compared with the rigorous Maliuzhinets' diffraction coefficients [30] which are based on Maxwell's equations.

2.3.2.1 Uniform theory of diffraction

The uniform theory of diffraction (UTD) method is applied for calculating the diffraction field for a perfectly (lossless) conducting wedge. It takes into account the diffraction in both shadow and line-of-sight regions, and provides smooth transition fields between these regions. Fig. 2-2 illustrates the diffraction around a corner of a building. The diffraction field at the observation point is calculated by [31]:

$$E_{UTD} = E_0 \cdot \frac{e^{-jks_1}}{s_1} \cdot D \cdot \sqrt{\frac{s_1}{s_2(s_1 + s_2)}} \cdot e^{-jks_2}, \quad (2-6)$$

where k is the wave number, E_0 is the initial source amplitude, and s_1 and s_2 are the distances from the diffracting edge to the source and field points, respectively. ϕ' and ϕ are the incident and diffraction angles for the 0-face and the n -face, respectively. D is the

diffraction coefficient depending on the polarization state, i.e., TE or TM wave. Note that the TE and TM waves refer to electric wave vectors that are perpendicular and parallel to the edge of the wedge, respectively. The diffraction coefficient can be expressed as:

$$D_{TE} = D_{TE}(L, n; \phi, \phi') = D_1 + D_2 + D_3 + D_4 \quad (2-7a)$$

and

$$D_{TM} = D_{TM}(L, n; \phi, \phi') = D_1 + D_2 - D_3 - D_4 \quad (2-7b)$$

where the components D_i ($i = 1, 2, 3, 4$) are given by:

$$D_i = D_i(L, n; \phi, \phi') = \frac{-e^{-j\pi/4}}{2n\sqrt{2\pi k}} \cot \gamma_i F(2kLn^2 \sin^2 \gamma_i). \quad (2-8)$$

$n\pi$ is the exterior angle of the wedge, $L = s_1 s_2 / (s_1 + s_2)$ for spherical wave incidence, and

$$\gamma_1 : \{ \pi - (\phi - \phi') \} / 2n$$

$$\gamma_2 : \{ \pi + (\phi - \phi') \} / 2n$$

$$\gamma_3 : \{ \pi - (\phi + \phi') \} / 2n$$

$$\gamma_4 : \{ \pi + (\phi + \phi') \} / 2n$$

In Eq. (2-8), $F(x)$ is the transition function and is defined as:

$$F(x) = 2j\sqrt{x} \cdot \exp(jx) \cdot \int_{\sqrt{x}}^{\infty} \exp(-jt^2) dt. \quad (2-9)$$

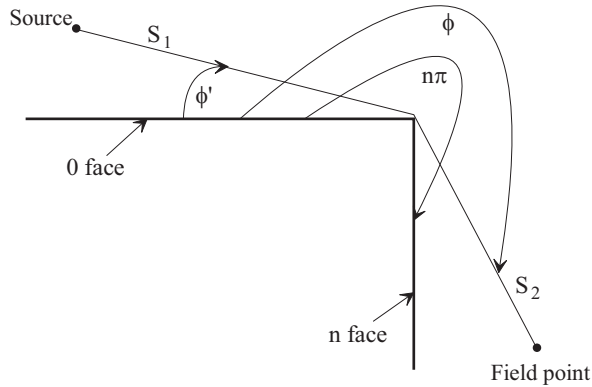


Fig. 2-2. Geometry for diffraction by a wedge.

2.3.2.2 Heuristic diffraction coefficients

Heuristic diffraction coefficients for lossy wedges have been proposed by Luebbers and Holm. In the case of these coefficients, the finite conductivity and the permittivity of the wedge are taken into account. The Luebbers' and Holm's diffraction coefficients are expressed as [32][33]:

$$D_L = D_L(L, n; \phi, \phi') = D_1 + D_2 + R_0 D_3 + R_n D_4 \quad (2-10)$$

and

$$D_H = D_H(L, n; \phi, \phi') = D_1 + R_0 R_n D_2 + R_0 D_3 + R_n D_4, \quad (2-11)$$

where R_0 and R_n are the plane wave Fresnel reflection coefficients for the 0-face and the n -face (see Fig. 2-2), respectively. Note that, for perfectly conducting surfaces, $R_{0,n}$ is -1 and 1 for TM and TE boundary conditions, respectively.

Comparison of different diffraction coefficients as a function of the mobile location around a corner at 60 GHz is shown in Fig. 2-3, where the wedge is considered to be of brick with material permittivity $\epsilon_r = 4.0 - j0.1$. It can be seen that the UTD diffraction coefficient is inaccurate (e.g., far away from Maliuzhinets' coefficient for TM wave) since it takes perfect conducting wedge into calculation. The Holm's diffraction coefficients are more accurate than the Luebbers' coefficients when comparing with the rigorous Maliuzhinets' diffraction coefficients. Therefore, the Holm's coefficients are recommended and used in field simulations in Chapter 4 of this work.

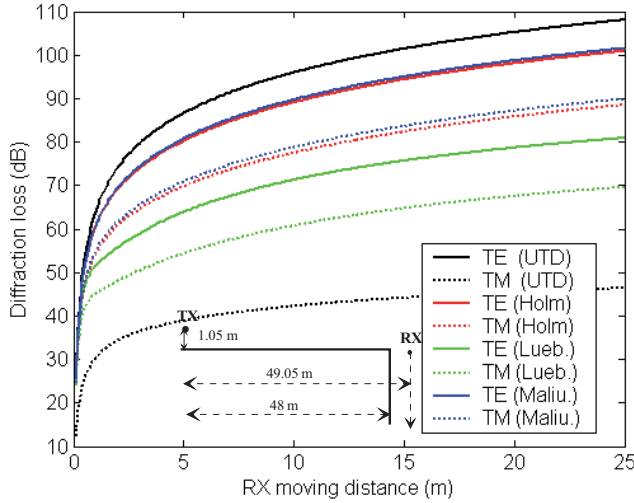


Fig. 2-3. Diffraction attenuation by different diffraction coefficients at a corner at 60 GHz.

2.4 Statistical modeling

Statistical modelling relies on extensive measurement data for characterizing channel properties. Statistical models and parameters can be derived and extracted from the measured channel impulse responses (IRs). A convenient MIMO model is the double directional channel model [34]. The polarimetric double directional model at time instant t can be expressed as:

$$h(t, \tau, \Omega_r, \Omega_t) = \sum_{i=1}^{N(t)} \begin{pmatrix} \alpha_i^{\theta\theta}(t) & \alpha_i^{\phi\theta}(t) \\ \alpha_i^{\theta\phi}(t) & \alpha_i^{\phi\phi}(t) \end{pmatrix} \delta(\tau - \tau_i(t)) \delta(\Omega_r - \Omega_{r,i}(t)) \delta(\Omega_t - \Omega_{t,i}(t)), \quad (2-12)$$

where N is the number of multipath components, τ denotes excess delay, $\Omega_{r,i}(t) = [\theta_{r,i}, \phi_{r,i}]$ and $\Omega_{t,i}(t) = [\theta_{t,i}, \phi_{t,i}]$ are the elevation and azimuth angles of arrival (AoA) and departure (AoD) of the i^{th} multipath component, respectively. The $\alpha_i^{\theta\theta}$, $\alpha_i^{\phi\phi}$, $\alpha_i^{\phi\theta}$, and $\alpha_i^{\theta\phi}$ denote the

path weights of the co- and cross-polarizations, and the Dirac delta function illustrates the plane wave model.

2.4.1 Statistical parameters

Statistical parameters are important and useful in system design: e.g., the number of paths (NP) greatly impacts time domain transmission techniques, rms delay spread (referred to DS hereafter) is used to determine the maximum transmission data rate of channel without equalization, and cross polarization discrimination (XPD) strongly affects the system capacity (as fading of different polarization is approximately uncorrelated) [13]. It should be noted that in this work, the statistical angular parameters are out of scope, due to the measurements for these having not been performed. However, the power angle profiles (PAPs) are measured in the 60 GHz-band DOA measurements.

2.4.1.1 Number of paths

The number of paths (NP) is estimated by counting the number of peaks of each PDP along the measurement route for the 60 GHz channel [P1]. For the UWB channel, it is difficult to extract the number of paths. Since the main forms of multipaths are single-dominant and diffuse paths, and the diffuse paths cannot be separated in practice. In this work, it is found that the distribution of the number of paths can be described with the Poisson distribution. Moreover, the number of paths in corridor environment is lower when compare with other environments like the open hall. This leads to a deviation from the Poisson distribution in the corridor environment. Also, this complies with the result in [22] that the distribution of the number of paths is governed by the Poisson distribution, and the discrepancy between the Poisson and empirical distributions is due to a relatively small number of paths, which increases the probability of clustering.

2.4.1.2 Delay spread

Rms delay spread (DS) is a measure of delay dispersion in the channel. It degrades the performance of communication systems and thus is of major concern in system deployment. DS is the square root of the second central moment of a PDP and expressed as [13]:

$$\sigma_{\tau} = \sqrt{\frac{\sum_{i=1}^N (\tau_i - \bar{\tau})^2 P_i}{\sum_{i=1}^N P_i}} \quad (2-13)$$

where the mean excess delay of multipath components (MPCs) is expressed as: $\bar{\tau} = \frac{\sum_{i=1}^N P_i \tau_i}{\sum_{i=1}^N P_i}$, N is the number of multipath delay bins obtained from each continuous PDP, and τ_i and P_i are the excess delay and corresponding power of the i -th delay bin, respectively.

It is found that DS depends on the size and structure of its environment, and a NLOS scenario generally results in increased delay spread in the channel [P1][P2]. The distribution of DS is log-normal when DS is expressed in logarithmic-scale. However, it is infeasible to compare DS s in the UWB and 60 GHz channels, as different power dynamic ranges as of 40 dB and 20 dB are chosen for the two channels. Note that a large dynamic range results in a larger DS in general [P1]-[P8].

2.4.1.3 Cross polarization discrimination

The cross polarization discrimination (XPD) is studied by using vertical and horizontal polarized antennas in the measurements. In multipath propagation channel, signals can be partially depolarized due to the polarization-dependent scattering in the channel. *XPD* is the traditional parameter for characterizing the amount of depolarization state in channel. It is defined as the ratio of received signals for co and cross polarizations in the measurements. In this work, *XPD* is studied for the 60 GHz corridor measurements where polarization measurements were performed. The notation of polarization is particularly complex in UWB channels because the cross polarization of both the channel and antennas can be frequency-dependent [12].

2.4.2 Statistical models

Power delay profile (*PDP*) is important in characterizing the channels' general properties. However, in practice, measured PDPs keep on varying along the mobile moving route due to the variation of the propagation channel for a specific environment. The average power delay profile (APDP) is a reliable estimate in characterizing the main features of the channel [35].

2.4.2.1 Average power delay profile (APDP)

The APDP is obtained by averaging the individual PDPs over a small scale area in an environment. In this work, APDPs in the UWB channel are obtained by averaging the individual PDPs over the 25 grid point at each measurement position, the average range being 10λ for the APDPs in the 60 GHz channel. A study shows that the single exponential decay law and/or power decay law can be used for characterizing general multipath (i.e., single-cluster) properties of a channel [36][37].

2.4.2.2 Saleh-Valenzuela (S-V) cluster model

The Saleh-Valenzuela (S-V) model [38] is used for characterizing multi-cluster properties of a channel generally. In the S-V cluster model there are four defining parameters, i.e., cluster decay rate (Γ), cluster arrival rate (Λ), ray decay rate (γ) and ray arrival rate (λ), as shown in Fig. 2-4. The conventional S-V model is expressed as:

$$h(t) = \sum_{l=0}^L \sum_{k=0}^{K_l} a_{k,l} \delta(t - T_l - \tau_{k,l}), \quad (2-14)$$

where L and K_l denote the number of clusters and the number of rays within the l^{th} cluster, T_l represents the arrival time of the l^{th} cluster, and $\tau_{k,l}$ is the arrival time of the k^{th} ray within the l^{th} cluster, relative to T_l . In the S-V model, both clusters and rays decay, i.e., the received signal amplitude β_{kl} obeys double exponential decay law:

$$\overline{\beta_{kl}^2} = \overline{\beta^2(0,0)} e^{-T_l/\Gamma} e^{-\tau_{kl}/\gamma}, \quad (2-15)$$

where $\overline{\beta^2(0,0)}$ describes the average power of the first arrival of the first cluster, Γ and γ being the decay rates of a cluster and a ray, respectively. The cluster and ray arrival times are given by the Poisson processes with distributions given by:

$$p(T_l | T_{l-1}) = \Lambda e^{-\Lambda(T_l - T_{l-1})} \quad (2-16)$$

and

$$p(\tau_{kl} | \tau_{k-1,l}) = \lambda e^{-\lambda(\tau_{kl} - \tau_{k-1,l})}, \quad (2-17)$$

where Λ and λ are the cluster and ray arrival rates, respectively.

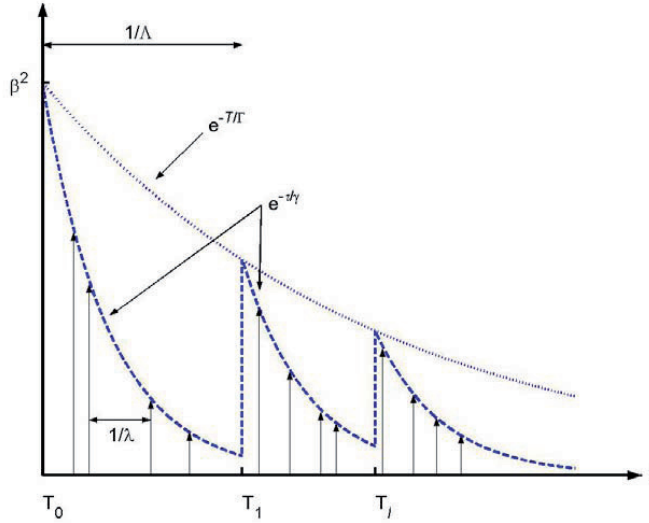


Fig. 2-4. The Saleh-Valenzuela (S-V) model.

2.5 UWB and 60 GHz channel measurements and data analysis

In this work, the UWB and 60 GHz channel measurements were performed in frequency and time domains, respectively. The frequency domain measurements can be done easily, but the measurement time is long. This results in limited measurement data for statistical analysis. The time domain sounder measurements are complicated but fast in collecting measurement data. Modeling of the propagation channel depends largely on measurement facilities, and this has influenced the selection of the characteristics of UWB and 60 channels that are studied in this work, as shown in Table 2-1.

Table 2-1. The UWB and 60 GHz channel characteristics studied in this work.

Channel	Measurements	Fading		Statistical properties		Ray-based models
		Large scale (Path loss & shadowing)	Small scale (multipath distribution)	Parameters	New models	
UWB	Frequency domain (VNA)	Yes	No	DS, APDP	Cluster	No
60 GHz	Time domain (Sounder)	Yes	Yes	DS, APDP, NP, XPD	Interdependency of characteristics	Yes

Channel parameters are affected by the selection of power dynamic ranges (DRs). For example, large dynamic range results in larger DS in general. In this work, 20 dB and 40 dB DRs are chosen for the 60 GHz and UWB channels. The DR value for the 60 GHz channel is very typical in traditional wideband-band systems. However, for the UWB channel the DR is not well defined in open literature. It was forced as 20 dB, 30 dB and 40 dB with general observation in [39]-[42]. In this work, 40 dB dynamic range (DR) is chosen by using the least square error fitting (LSEF) to obtain channel path loss models for the UWB channels [P4]-[P7]. It should be noted that the antenna gains are eliminated directly from the measurement data in processing the measurement data in this work. This is because the directions of paths are unknown, and thus it is not possible to remove the antenna pattern effects from the measurement data. However, the measurement data clearly includes the effects of antenna patterns, e.g. a directive antenna typically limits the number of paths.

2.5.1 UWB measurement setup and environments

In UWB measurements, a vector network analyzer (VNA) was used to sweep a frequency band of 3-10 GHz, which was segmented into two pieces of 3-6.5 GHz and 6.5-10 GHz for enhancing delay range. Channel impulses were obtained by weighting with a Hamming window prior to inverse Fourier transform of the frequency domain measurement data. Measurements were performed in a hall (LOS), a meeting room (NLOS) and corridors for both the LOS and NLOS scenarios. In each measurement environment, the TX was fixed at a certain position while the RX was placed at different positions approximately 1 m apart from each other. Spatial averaging was adopted (i.e., at each position the measurement was performed at 25 grid points with 100 mm spacing) for removing the small scale fading effect of the channel. In the measurements, two identical biconical horn antennas (with 1 dB gain) were used at the TX and RX, and the antennas were set to the same height of 1.5 m above the ground. Detailed information on UWB measurement parameters can be found in Table 1 of [P4] and environments in Figs. 1-3 of [P5], respectively.

2.5.2 The 60 GHz propagation measurements

The radio channel sounder of the Helsinki University of Technology (the Aalto University School of Science and Technology currently) has been developed for a large range of 2, 5.3 and 60 GHz frequency bands [43]-[45]. The 60 GHz radio channel sounder [45] measurements were performed for continuous-route (CR) and direction-of-arrival (DOA) measurement campaigns, for channel statistical modeling and for propagation mechanism studies. The CR measurement locations chosen were typical indoor spaces, such as a hall and a corridor for both the LOS and NLOS scenarios. Both directional horn (gain 22.7 dB) and omnidirectional biconical horn (gain 5 dB) antennas were used in the CR measurements. The DOA measurements were performed in a room (LOS) and a corridor (NLOS). In the DOA measurements, the TX antenna was an omnidirectional biconical horn, and the RX antenna was a direct horn, which was rotated in the azimuth plane from 0° to 360° at each measurement position. The TX and RX antennas are set at the same height in the range of 1.25-1.65 m above the ground. The transmission bandwidths are 60 MHz and 100 MHz in the measurements. Detailed information on 60 GHz measurement parameters and campaigns can be found in Table 1 of [P1].

3. ULTRAWIDE-BAND (UWB) RADIOS IN THE MICROWAVE RANGE (3-10 GHz)

3.1 Introduction

The UWB propagation channel has been studied for several years [46]-[51]. The UWB radios in the microwave frequency range of 3.1-10.6 GHz were proposed for commercial applications by FCC in February 2002. Since the specified UWB spectrum overlaps with other radio systems operating in its range and obeying different rules, low transmission power spectral density (PSD) of -41.3 dBm/MHz was specified by FCC in order to reduce interference with other existing radio services. However, the low PSD poses design challenges for UWB system because the other services sharing the same band are likely to have a much higher transmission power than the UWB systems. Multiband (MB) approach is an attractive solution for preventing the potential interference problem in the UWB systems [51]. In this work, UWB channel frequency dependency properties are studied by examining propagation characteristics in the MB channels [P6][P7].

3.2 Clustering channel characterization

For system design, especially in the context of system standardization, site-independent models are often required. The S-V cluster model is proposed in IEEE 802.15.3a and 4a standardizations for UWB systems [12]. In this work, the indoor UWB channels are classified as single- and multi- cluster channels. This is because a single-exponential decay function and a modified multi-cluster model can be used for characterizing the two cluster channels [P5].

3.2.1 Single-cluster channel

The measurement hall (LOS) and meeting room (NLOS) represent general propagation environments, where the azimuthal angular distribution of MPCs is fairly uniform over the range of $(0, 2\pi]$. It is found that the LOS hall and NLOS room can be classified as single-cluster channels, since single exponential power decay function (PDF) can be used for characterizing channel properties [P5].

3.2.1.1 Single-exponential power delay profile

Fig. 3-1 shows an example of a PDP in the LOS hall. It is seen that the LOS component is about 20 dB higher than other paths. This indicates that the LOS path dominates over the other MPCs and radiowaves propagate like in free space. Note that in the NLOS case the signals propagate with a larger decay rate, which indicates severe fading in the environment. The single-exponential power decay function can be modelled as:

$$P(\tau) = P_0 \cdot 10^{-\alpha\tau}, \quad (3-1)$$

where P_0 denotes the initial power and α is the power decay rate.

3.2.1.2 Forms of multipath components

The main forms of the multipath components (MPCs) are *single dominant* and *diffuse paths*, which are associated with specular and diffuse (scattering) reflections in the environments. This is because scattering produces lots of relative weak MPCs results in diffuse paths (due to roughness of walls and effects of furniture) in the UWB channel. The single dominant paths

can be easily identified from both power level and width as shown in Fig. 3-1. Specifically, the power level of the single dominant paths reaches at least 5 dB higher than the surrounding diffuse paths, and the width is about several nanoseconds (3-8 ns). This is due to the fine resolution of UWB systems. For example, over a spatial distance of 300 mm the position of a single echo may move up to $300\text{mm}/c_0 = 1$ ns (c_0 is the speed of light in free space), which is several times of the width of a single echo (the resolution of the measurement system) of about 140 ps in the UWB channel.

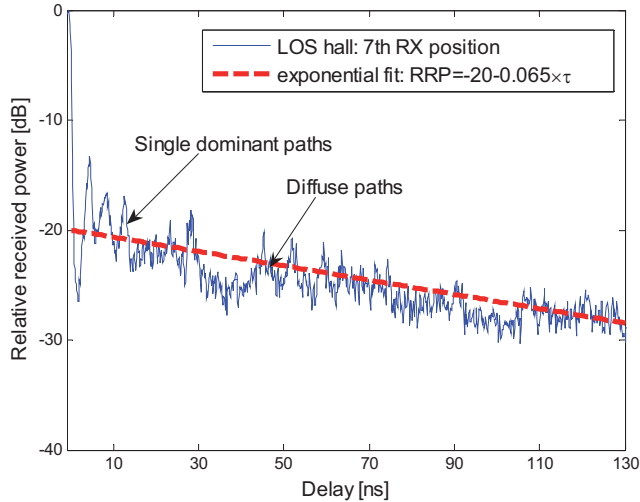


Fig. 3-1. Single-cluster channel characterization for the LOS hall.

3.2.2 Multi-cluster channel

Multiple clusters are observed in the corridor environment for different measurement scenarios. Note that in the corridor environment, the MPCs are associated with a limited angular spread since reflections can be mainly occurred on the two sides of the walls and doors of the corridor.

3.2.2.1 Multi-cluster specification

Identification and specification of clusters is the first step and a very crucial one in extracting cluster parameters. In this work, multiple clusters are specified as the groups of multipaths, with power range ≥ 20 dB and separation ≥ 25 ns, for extracting the multi-cluster parameters and for comparing with the single-dominant paths (power and delay ranges of 5 dB and 3-8 ns) in single-cluster channels. Clusters can be identified based on the changes of amplitude and delay in PDPs at different RX positions in the LOS corridor for closed-door measurements. Fig. 3-2 shows the measured clusters in the LOS corridor for the closed-door case when the TX-RX separations are of 9 m and 13 m (plotted with a -40 dB offset).

The A cluster is regarded as the direct-path since at the two RX positions the delays are of 30 ns and 43 ns which coincide with the real environment. Clusters B and C are the reflected waves from the two corridor doors, i.e., the C-door and W-door, respectively. For instance, when the RX moves from 9 m to 13 m, the delay of cluster B decreases and the delay of cluster

C increases both by 13 ns, which coincides with the real propagation path lengths. Moreover, the structures of the clusters are quite similar, i.e., each cluster comprises one dominant path followed by some other dominant paths and/or diffuse paths. Thus, a heuristic approach to clusterization applies: a cluster is formed by direct or reflected waves from one piece of reflector with a large size and smooth surfaces. This observation naturally leads to a result that the number of clusters is constant over all positions for the same measurement scenario in the corridor measurements.

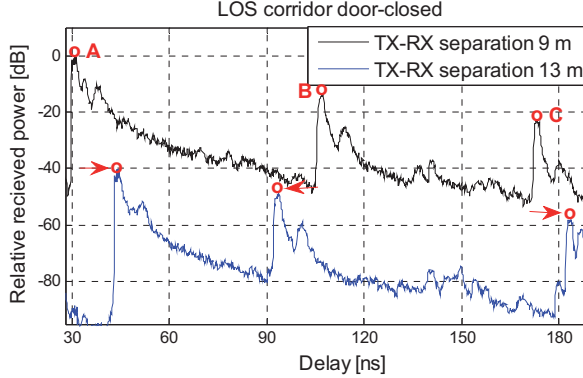


Fig. 3-2. Clusters in the LOS corridor in the *closed-door* case when the TX-RX separations are 9 m and 13 m (plotted with -40 dB offset).

3.2.2.2 A modified multi-cluster model

Clusters do not necessarily follow exponential-decay (i.e., the classical S-V mode), but can be better fitted with a power-decay law. This is the so-called modified multi-cluster model hereafter for the corridor measurements in this work. For the purpose of comparison, Fig. 3-3 shows the measured clusters fitted with the S-V model (upper curve) and the modified multi-cluster model (lower curve, plotted with -80 dB offset) in the LOS corridor for the closed-door case when the TX-RX separation is 9 m. The modified multi-cluster model is expressed [P5]:

$$P(\tau) = \sum_{n=1}^N P_n (\tau - \tau_n)^{-\alpha_n}, \quad (3-2)$$

where N is the number of clusters, and P_n , α_n , n denote the power, decay rate and starting point of the n th cluster, respectively.

It is seen that the proposed multi-cluster model (lower curve) fits better with the measurement data when compared with the S-V model (upper curve) with eye-inspection in Fig. 3-3. Fig. 3-4 shows the parameters of the modified cluster model for the same measurement data (of Fig. 3-3). The parameters in the proposed cluster model of Eq. (3-2) physically indicate clustering properties in channel. Specifically, the mean power $\bar{P} = 12$ dB indicates the average reflection loss from corridor doors. The cluster decay rate is almost constant ($\bar{\alpha} \approx 2$) indicating that the clusters are formed by the same propagation phenomenon (i.e., reflection from corridor doors) in the environment. The cluster arriving time is about 70 ns corresponding to 21 m, which is about the length of the LOS corridor. Note that in the NLOS corridor the parameters of the modified cluster model have larger delay and decay rate. However, explaining the cluster parameters as the propagation phenomena is not clear in this case.

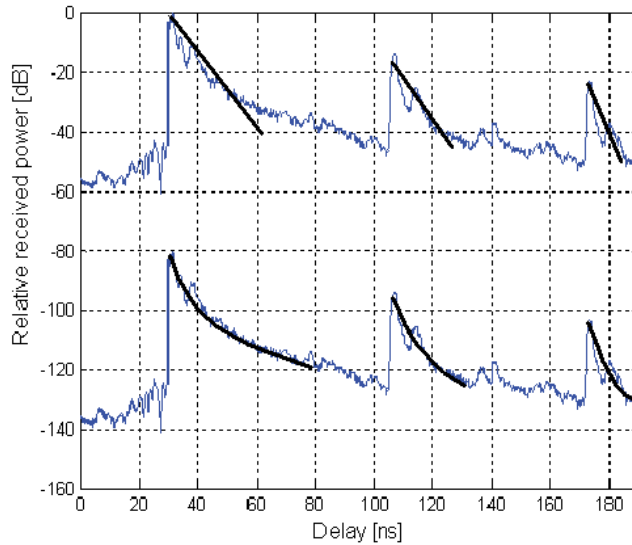


Fig. 3-3. Comparison of the S-V model (i.e., exponential power decay, upper curve), and the proposed multi-cluster model (lower curve, plotted with -80 dB offset) for the closed-door LOS corridor measurement data when the TX-RX separation is 9 m.

It should be noted that in the S-V model, only the two parameters of clusters Γ and Λ , (but not the two parameters of rays γ and λ) can be extracted from the measurement data, since the diffuse paths (the main form of multipaths) cannot be separated from measurement data in practice. It can be shown that the two cluster parameters, Γ and Λ are almost the same in the LOS corridor for the open- and closed- door measurements. This indicates that the two cluster parameters depend mainly on the building structure (e.g., corridor) of the environment.

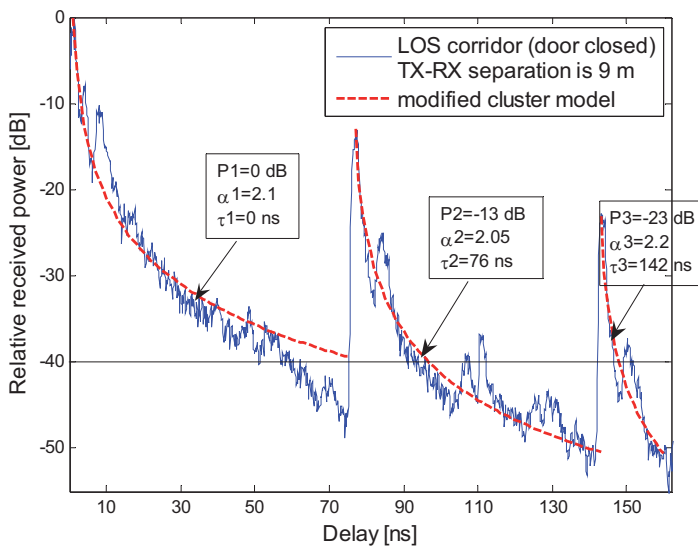


Fig. 3-4. The modified cluster model used for characterizing the multiple clusters in the LOS corridor for closed-door measurements when the TX-RX separation is 9 m.

3.3 Frequency dependence of UWB channel

Due to the large bandwidth of the UWB channel, the characteristics may exhibit frequency dependency. In this work, the frequency dependency of the UWB channel is investigated by examining propagation characteristics in the multi-band (MB) channels. The MB approach is accomplished by dividing the single-band (SB, the entire band 3-10 GHz) into 14 different frequency bins, as shown in Fig. 3-5.

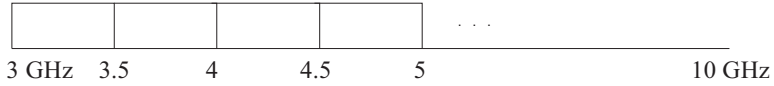


Fig. 3-5. The multiband radio channels.

Frequency dependencies of channel delay spread, path loss exponent and shadowing STD are investigated [P6][P7]. It can be shown that DS can either increase or decrease in the multiband channels: the PL exponent does not depend on frequency, but shadowing STD has a clear tendency of increasing with frequency in general. As an example, Fig. 3-6 shows the frequency dependency of the shadowing STD in the LOS hall and corridor environments. Comparisons of multipath components in the MB and SB channels are shown in Fig. 3-7, where only the lowest

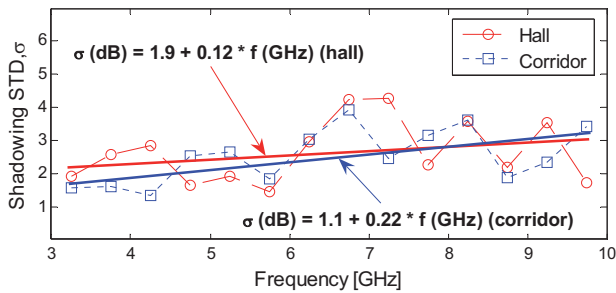


Fig. 3-6. Frequency dependencies of the shadowing STD in the LOS hall and corridor.

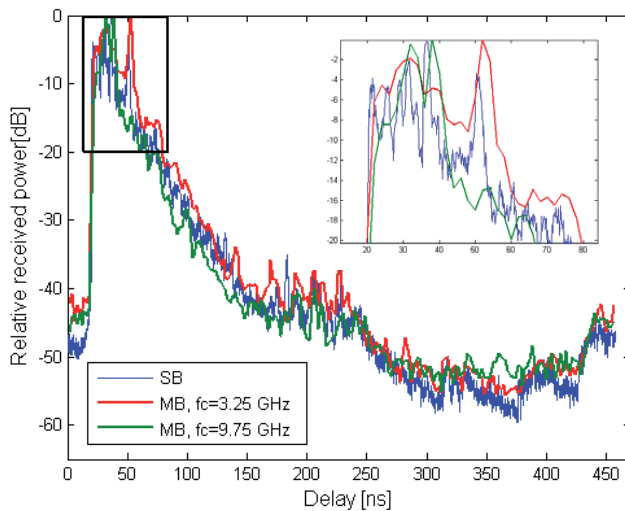


Fig. 3-7. Comparison of PDPs in the single-band and multi-band channels in the NLOS room.

and highest frequency bins with the center frequencies at 3.25 GHz and 9.75 GHz are selected, since the PDPs are quite similar for the 14 different multi-band frequency bins. It can be seen that the more visible dominant multipaths in the case of SB are more visible than in the case of MB. The dominant multipaths also appear at different delays and have different attenuations. This indicates that scattering depends on the different center frequencies of channels.

3.4 Bandwidth dependence of UWB channel

Bandwidth dependence of the UWB channel is also examined for channels having a common center frequency $f_c = 6.5$ GHz, when the bandwidths are incrementally increased around f_c in 500 MHz steps as shown in Fig. 3-8. As an example, the bandwidth dependencies of the PL exponent and the shadowing STD of the UWB channels are shown in Fig. 3-9. It is seen that the path loss exponent is almost constant and the shadowing STD decreases with bandwidths. This indicates that signals with large bandwidth exhibit less variation in the received signal power than those in the smaller bandwidth channel. Note that this result is used for modeling the channel fading margin in 60 GHz UWB systems in Chapter 5.

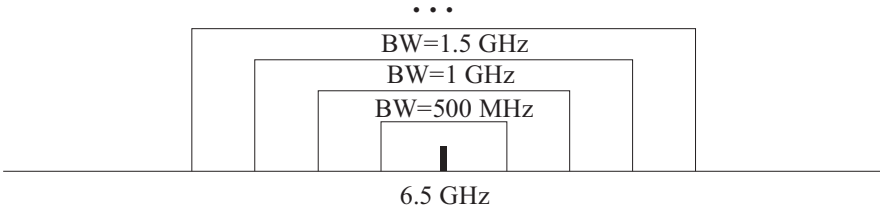


Fig. 3-8. The channels with different bandwidth.

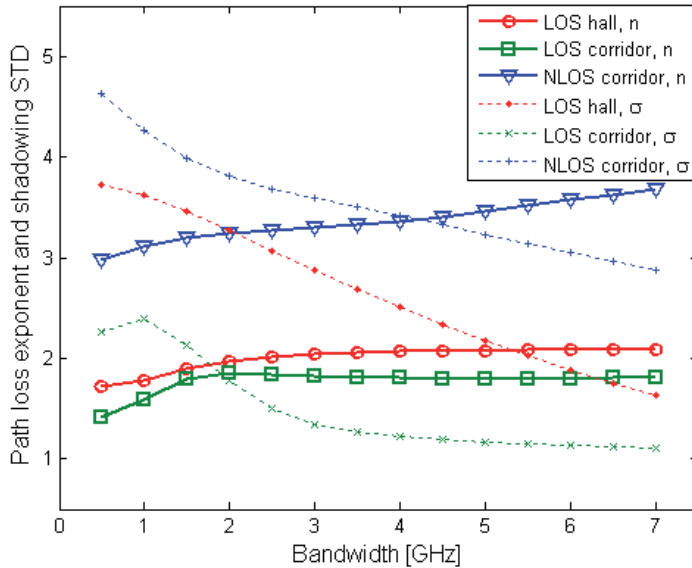


Fig. 3-9. Path loss exponent and shadowing STD in the channels with different bandwidths.

3.5 Fading robustness of UWB signals

Ultra wide bandwidth leads to frequency or multipath diversity, or UWB signal is robustness to multipath fading. This is indeed seen in the measurements and shown in Fig. 3-10, where the slope of the UWB signal (NLOS room data) is comparable with 8-branch diversity distribution of standard Rayleigh narrowband signal with maximal ratio combining. Whereas, UWB channel provides a shadow fading improvement relative to narrow-band channel (or shadowing STD decreases with bandwidth as already shown in Fig. 3-9). For example, the shadow fading margin is less than 4 dB with 90 % link success probability for a 500 MHz UWB channel [P7].

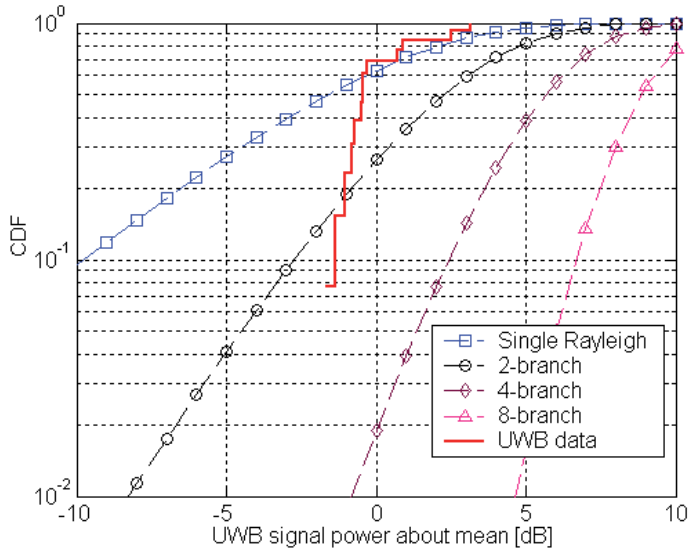


Fig. 3-10. Comparison between the UWB signal and the standard Rayleigh narrowband signal with different diversity order and maximal ratio combining.

3.6. Findings about UWB propagation channels in this work

Previous studies on UWB propagation channels are mainly on analysis of statistical parameters [46]-[51]. Cluster parameters for the conventional S-V model in the UWB channel are extracted in [53][54].

In this work, UWB channel statistical parameters are analyzed, and some new scientific results are presented in addition. Specifically, frequency and bandwidth dependencies of propagation in the 3-10 GHz UWB range are investigated [P6][P7]. The UWB propagation characteristics are modeled as functions of frequency, which are useful for the design of radio systems. A modified cluster model of the UWB channel is proposed [P5]. The model fits better with the measurement data, and the parameters in the model physically indicate cluster properties of the propagation channel. The general properties of UWB and 60 GHz channels are compared based on the experimental channel measurements [P4]. The findings about UWB propagation channels [P4]-[P7], enable analysis of a high throughput 60 GHz UWB radio system [P8] later in Chapter 5.

4. MILLIMETER-WAVE (60 GHz) BAND

4.1 Introduction

The 60 GHz band has emerged as one of the most promising candidates for gigabit indoor wireless communication systems. The band has been proposed for > 1 Gbps and < 10 m range WPAN applications in the IEEE 802.15.3c [55]. The 60 GHz-band technology offers various advantages over current or existing communications systems: 1) it can be viewed as a shift version of the UWB radio due to the large available bandwidth (as a rule of thumb, the available bandwidth is about 10% of centre frequency), 2) small size antenna arrays or MIMO systems can be developed. Moreover, the current state-of-the-art 60 GHz circuit technologies enable the development of low cost radio devices for the market [56][57].

The 60 GHz propagation channel has been studied for many decades [58]-[61]. Previous studies of the 60 GHz propagation channel mainly focused on channel statistical parameters and the measurements were done in the frequency domain [62]-[68]. Moreover, little information on the direction-of-arrival (DOA) measurements is available [68]. Thus, the role of different radio-wave propagation mechanisms is not very well known in the 60 GHz band. In this work we investigate the propagation issues of: 1) radiowave propagation mechanisms, 2) interdependencies of different characteristics with channel delay spread, 3) ray-based models and 4) multipath power distributions in indoor corridors in the 60 GHz band. The investigation of these issues is based on experimental channel measurements performed in various indoor environments for direction-of-arrival (DOA) and continuous-route (CR) campaigns [P1].

4.2 Mm-wave propagation mechanisms

The DOA measurements can clearly demonstrate a strong relation between multipath channel structure and propagation environments [P1]. Fig. 4-1 shows the DOA measurement campaign of 60 GHz propagation channel measurements. It is worth to note that *person blocking effect* was also measured in the DOA measurements [2] when a person blocked the LOS path (the path between TX and RX when it was placed at position 1 in Fig. 4-1). From the DOA measurements, the following conclusions can be made:

- Direct path and the first-order reflected waves from smooth surfaces form the main contributions in LOS propagation environments.
- Diffraction is a significant propagation mechanism in NLOS cases.
- Transmission loss through concrete or brick walls is very high. Person blocking effect is about 20 dB in the 60 GHz frequency band.

4.3 Ray-based models in indoor corridors

Ray-based models are proposed for the LOS and NLOS corridors where polarization measurements were done [P3]. Note that both horn (22.7 dB) and omni-directional biconical horn (5 dB, denoted as omni hereafter) antennas were used in the corridor measurements.

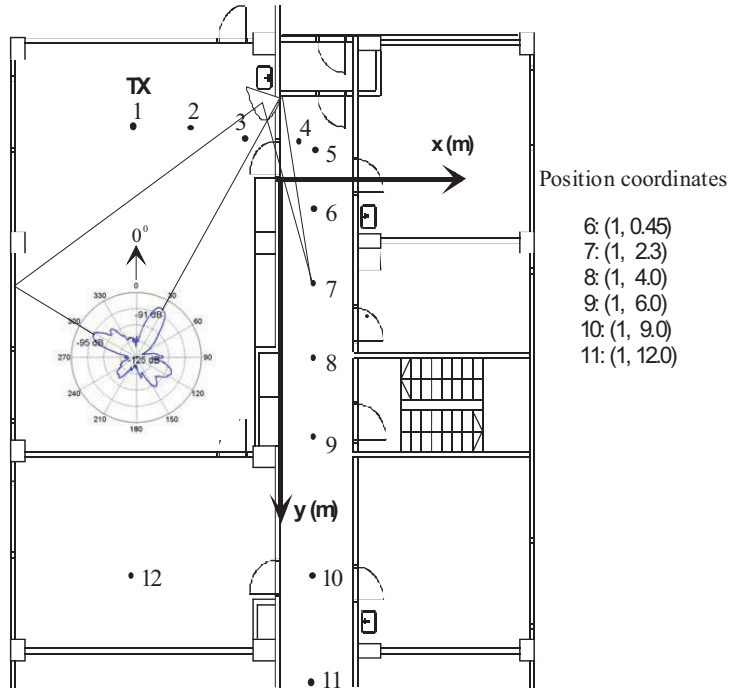


Fig. 4-1. The DOA measurement campaign.

4.3.1 LOS corridor

The proposed multi-ray models for the LOS corridor measurement data for vertical polarization (VP) are shown in Fig. 4-2, where the 5 rays are associated with the LOS path plus four first-order reflections, and the 9 rays refer to the five rays plus four second-order reflections from the two walls, ground and ceiling, respectively. It can be seen that the 9-ray model fits better with the measurement data than the 5-ray model. It is worth noting that using more than 9 rays does not improve the result. In other words, there is a convergence for number of rays. This is expected, since each reflection decreases the power of the ray essentially, and the high-order reflections with less grazing angles of incidence have stronger attenuation.

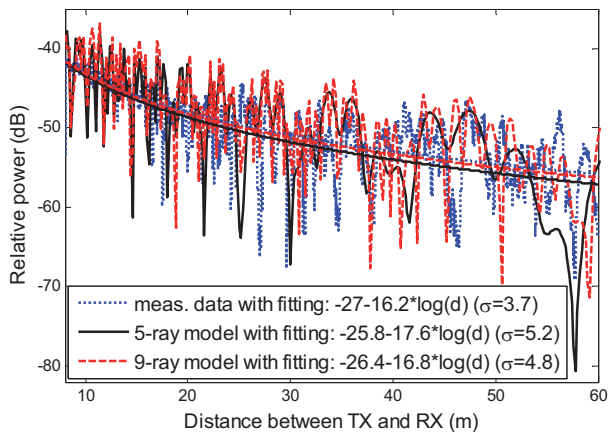


Fig. 4-2. Ray-based models in the LOS corridor for VP measurements.

4.3.2 NLOS corridor

The Holm's diffraction coefficient is used in the field simulation, since the Luebbers diffraction coefficient overestimates signal strength in the deep shadow region [69]. For the NLOS corridor different ray structures are proposed as shown in Fig. 4-3. Specifically these are the one-ray (diffracted from each of the two wedges), two-ray (diffracted from the two wedges), four-ray from one wedge (diffracted, diffracted-reflected, reflected-diffracted and reflected-diffracted-reflected), and eight-ray (doubled from the four rays) from the two wedges structures. As an example, four rays from the inner-wedge (close to TX) are shown at the top of Fig. 4-3. It should be noted that the diffraction from the inner-wedge is very small. Thus the curves of the two diffracted rays and that of the single diffracted ray for the outer wedge are practically the same. It is seen that the eight-ray model is in good agreement with the measurement data in both the average power level and signal variation. However, the model of diffracted rays (the two-ray model in Fig. 4-3) is accurate in characterizing the average power decay of a signal in the environment.

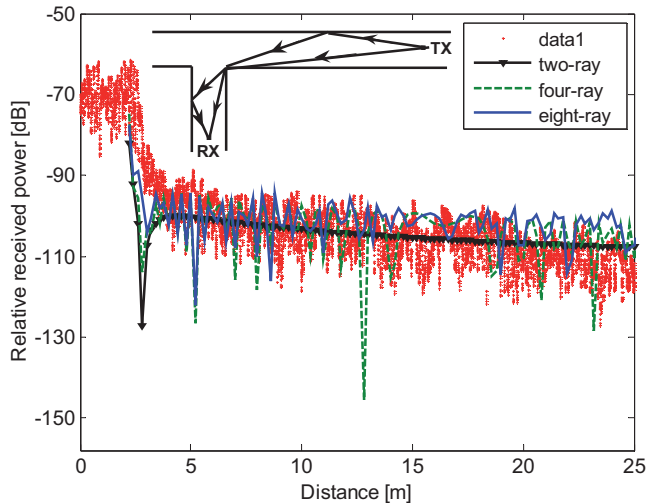


Fig. 4-3. Comparison of the proposed models and measurement data in the NLOS corridor.

4.4 Multipath power distributions

A key assumption in the implementation of Rayleigh and Rice distributions is that the channel itself does not change over small local area. However, in practice, the mobile radio channels are varying significantly. The channel seems to be directly related to the transitions from the Rayleigh or Rice distribution in local areas to other distributions in global areas. This is illustrated by selecting three LOS mobile routes in this work: the LOS corridor route (horn-omni), and two LOS routes (TX1 and TX2) in the hall environment as shown in Fig. 4-4. The three LOS routes are denoted as varying, dynamic and static channels, respectively. Since both the LOS path (decreases) and other multipaths (increase at further distances where paths with nearly grazing angle of incidence) are changing along the LOS corridor route. In the hall measurements, the LOS path decreases (power-distance law) along the TX1 route, and the other multipaths remain unchanged: the TX2 route is almost symmetric (both the LOS path and the mean of the scattered multipaths have essentially constant powers along the route).

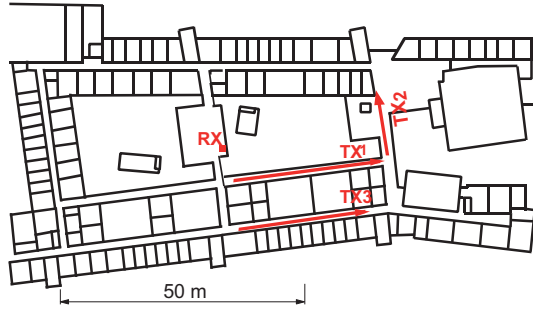


Fig. 4-4. The dynamic (TX1) and static (TX2) LOS routes and NLOS (TX3) route in the hall.

4.4.1 Distributions in mobile radio channels

Fig. 4-5 shows the multipath power distributions for the three LOS mobile channels. It is interesting to see that the static, dynamic and varying LOS mobile routes can be described by weak-Rice ($K = 3$ dB), Rayleigh and negative-Rice K distributions, respectively. Therefore, the following conclusions are made: 1) the mobile radio channel suffers from very severe fading (e.g., weak Rice K -factor is used for describing the static LOS channel), 2) Rice distribution may degrade to Rayleigh distribution when the LOS signal becomes weaker and/or the local mean of the multipath components becomes stronger, 3) negative Rice K -factor is used for describing the varying LOS mobile channel.

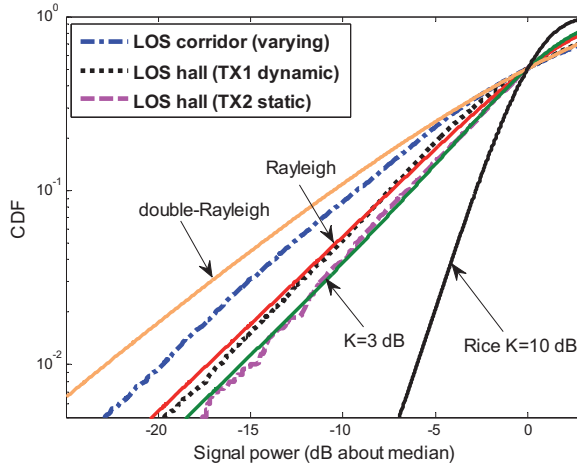


Fig. 4-5. Multipath power distributions in three LOS mobile radio channels.

4.4.2 Rayleigh and double-Rayleigh distributions

Rayleigh and double-Rayleigh distributions form the bounds for both the LOS (horn-onmi) and NLOS corridor data [P3] as shown in Fig. 4-6 (a). This implies that a combination of Rayleigh and double-Rayleigh signals can characterize the measurement data. This is indeed seen in computer simulations with different values of α , which is also shown in Fig. 4-6 (a). Therefore, we can conclude that the Rayleigh fading and double-Rayleigh fading are the most dominant ones compared to high-order Rayleigh fading. Note that the particular phenomenon that the LOS corridor data falls between the Rayleigh and double-Rayleigh distributions, can

be explained by the proposed multi-ray models in the environment. The signal consists of several multipaths like in the normal Rayleigh fading case, but due to narrow angular distribution at far distances in the LOS corridor the fading (or correlation) is clearly larger than in the normal case.

4.4.3 Multiple-Rayleigh distribution

As for the LOS corridor case, the vertical polarization (VP) and horizontal polarization (HP) measurement data show more variations than the horn-omni measurement data as shown in Fig. 4-6 (b). The reason might be that in the former case fewer paths were received than in the latter. Here it should be noted that the measurement data includes the effects of antenna patterns and a directive antenna typically limits the number of paths. However, as the directions of the paths are unknown, so it is difficult to remove the antenna pattern effects from the measurement data. The multiple-Rayleigh distribution can fit measurement data very accurately. It is encouraging to use this type of distribution, as it does not require details of the material properties and physical processes of propagation, and has a very good prediction accuracy. Moreover, the multiple-Rayleigh distribution has a clear theoretical explanation and is easy to implement in computer simulations.

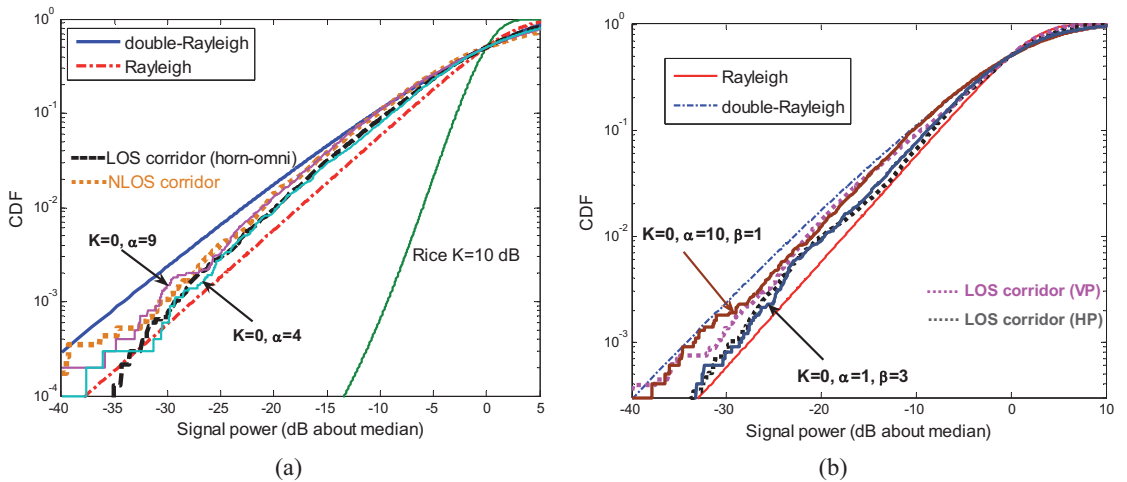


Fig. 4-6. (a) Rayleigh and multiple-Rayleigh distributions form bounds for both the LOS and NLOS corridor data, (b) Multiple-Rayleigh distribution vs. VP and HP measurement data in the LOS corridor.

4.5 Interdependence of channel characteristics

The interdependencies of different channel characteristics with delay spread (DS) are important in wireless communications systems [70]. In this work, the interdependences of path loss, shadowing, number of paths, Rice K -factor and cross polarization discrimination (XPD) with channel rms delay spread (DS) are investigated. As an example, Fig. 4-7 shows the relationship between the path loss and DS for the LOS corridor and hall. It is seen that an upper-bound model of delay spread and path loss can be developed. The model is useful in estimating the worst case of DS at a given path loss. In this work, the following general conclusions are made [P1][P2]:

- An upper-bound exponential model of path loss and delay spread can be developed.
- There is a negative cross-correlation between shadow fading and delay spread is found.
- A linear relationship between the number of paths and delay spread exists.
- The Ricean K-factor increases with the increase of DS in the channel.
- A low correlation property exists between the XPD and delay spread.

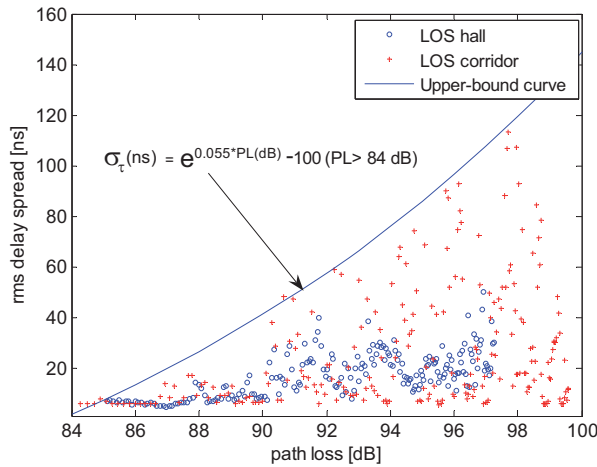


Fig. 4-7. Relationship between the path loss and the delay spread in the LOS corridor and hall.

4.6 Characteristics of mm-wave propagation signals

Mm-wave propagation signals suffer from very severe fading: e.g., in an environment for the same TX-RX separation distance there is always a 22 dB higher PL at 60 GHz than for example at the lower band of 5 GHz. Fig. 4-8 shows the path loss models in the 60 GHz propagation channels [P1]. It is interesting to note that shadow fading is increasing along the LOS corridor route. This can be explained by the proposed multi-ray models. At small distances, the significant LOS signal suppresses the effect of multipaths. At large distances, more strong multipaths with nearly grazing angle of incidence are received leading to larger variation of signal power or shadow fading in the LOS corridor [P3].

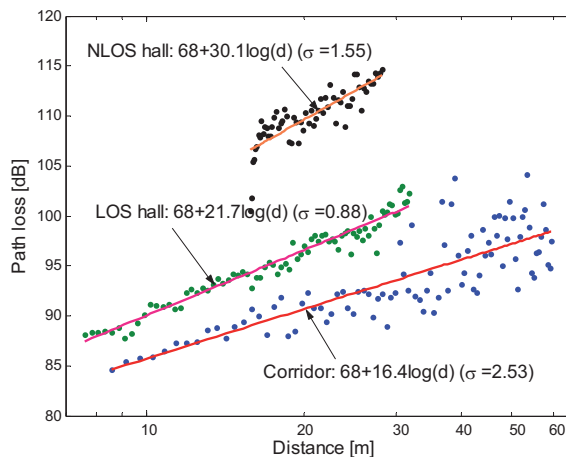


Fig. 4-8. Path loss models in the 60 GHz propagation channels.

Mm-wave signals are traceable. This can be illustrated with the received powers in NLOS corridors shown in Fig. 4-9, where two NLOS corridors denote the NLOS corridor route and the NLOS route in the hall. When denoting P_L as the received power along a LOS route d_L , L_{tran} as the transition loss in the cross corner, m as the decay exponent of the diffracted power along the NLOS corridor route d_{NL} , the received power can be expressed as [P3]:

$$P_r(d) = P_L(d_L) - L_{tran} - 10m \log(d_{NL}). \quad (4-1)$$

It is seen that the decay exponents of power in the two NLOS corridors of the corridor and hall environments are $m_{cor} = 0.8$ and $m_{hall} = 0.5$, which are much smaller than the path loss exponent in free space ($n = 2$). This indicates that diffraction is the main propagation phenomenon and that radio waves propagate in a guided fashion in the NLOS corridors. Note that the transition loss depends on the wedge size, structure, environment and frequency [71].

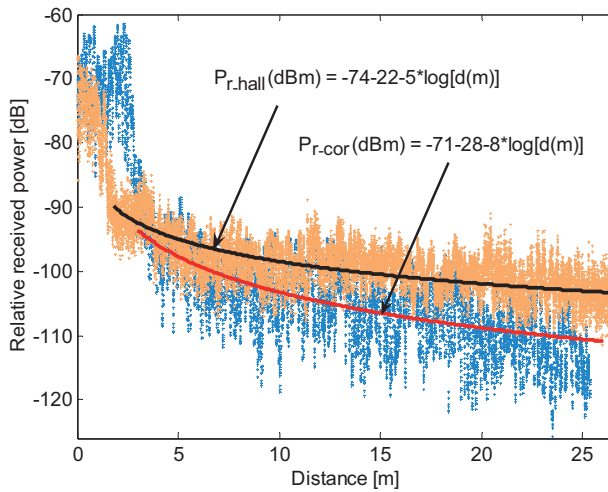


Fig. 4-9. Empirical models in the NLOS corridors.

4.7 Findings about 60 GHz propagation channels in this work

Previous studies of 60 GHz propagation channel are mainly focused on statistical parameters, and the measurements in those studies were performed in the frequency domain [58]-[67].

In this work, the 60 GHz propagation channel's statistical parameters are analyzed, additionally, some new scientific results are presented. More specifically, the 60 GHz propagation mechanisms are studied based on DOA measurements. An important finding is that diffraction can be a significant propagation mechanism in the NLOS propagation environments [P1]. This is different from the prediction in other literature according to which diffraction is generally ignored in the millimeter-wave frequency range [72][73]. From the continuous-route (CR) measurements, the interdependencies of different channel characteristics with delay spread were investigated [P1][P2]. They are important in predicting channel parameters from one another. Ray-based models in LOS and NLOS indoor corridors are proposed [P3] and multipath power distributions in indoor corridors are studied first time [P3]. The findings about 60 GHz propagation channels [P1][P2][P3] are useful for analysing the high data rate of 60 GHz UWB and MIMO radio systems in Chapter 5 [P8].

5. PERFORMANCE AND CAPACITY ANALYSIS OF 60 GHz UWB AND MIMO SYSTEMS

5.1 Introduction

The large available bandwidth makes the 60 GHz-band UWB system attractive for gigabit indoor wireless communications [74]. However, path loss is high in the 60 GHz-band, and increasing of bandwidth will lead to high noise power in the system. For example, noise power is 18 dB higher with a $B = 7$ GHz UWB channel than with a $B = 100$ MHz narrowband channel (when antenna noise temperature is $T = 290$ K). Though it is possible to use high gain antennas to compensate for the high loss at mm-waves, the drawbacks of such antenna systems are obvious: 1) they suffer from poor flexibility and limited mobility, 2) the narrow-beam signal of a high gain antenna can be easily blocked, which is a common concern in design of indoor multipath environments. MIMO systems are the key towards future gigabit wireless systems [75]. They provide the parallel channels in which independent information streams can be transmitted between TX and RX in the same frequency band without extra power. Thus the system capacity is increased greatly.

5.2 Channel capacities

For a SISO or an UWB channel, the maximum capacity (C) can be computed from the Shannon capacity theorem, which is expressed as a function of channel bandwidth (B) and signal-to-noise ratio (S/N) as:

$$C_{SISO} = B \log_2(1 + S/N). \quad (5-1)$$

In MIMO the spatial multiplexing (SM) is one natural potential for providing high channel capacity [76]. The maximum SM gain can be obtained by implementing MIMO configuration with equal number of TX and RX antennas, i.e., $N_T = N_R = N$ [77]. For the case that MIMO channel is known at RX but unknown at TX, assuming all antenna signals are spatially uncorrelated, the maximum capacity in the MIMO channel with a given bandwidth B is:

$$C_{MIMO} = B \log_2 \det \left(I + \frac{\rho}{N_T} HH^+ \right), \quad (5-2)$$

where I is the identity matrix, ρ is the average SNR, H is the normalized channel matrix, and '+' denotes the transpose-conjugate.

To perform a basic feasibility study for the 60 GHz UWB channel, B is chosen as 2 GHz and SNR is considered as 10 dB, which is a common value for a high rate 60 GHz channel [78][79]. As there is no agreement on 60 GHz MIMO standards yet, the bandwidth is considered as $B = 100$ MHz as it is a typical value in traditional wideband 60 GHz SISO channel measurements [P1].

5.3 Radio link budgets

In wireless communication systems, the performance and robustness is often determined by SNR from radio link budget:

$$SNR = P_t + G_t + G_r - \overline{PL} - FM - N_0 - IL, \quad (5-3)$$

where P_t is the transmitted power, G_t and G_r are the transmitter (TX) and receiver (RX) antenna gains, \overline{PL} and FM denote the mean path loss and fading margin in channel, N_0 is the total noise power at TX, and IL denotes the implementation loss of the system.

Transmission power is often specified in regulations. Based on the European regulation for the 60 GHz band, P_t is chosen to be 20 dBm [14]. The other system parameters are set as practical values, i.e., $IL = 6$ dB and noise figure $NF = 6$ dB for calculating $N_0 = 10 \log_{10}(kTB) + NF$, where k is the Boltzmann's constant and T is the standard noise temperature at $T = 290$ K.

In the 60 GHz UWB channel two path loss models are employed. Specifically, a LOS model including blocking effect (BE) and a NLOS path loss model, and they are expressed as: $PL_1(dB) = 68 + 18 \log(d) + BE$, where $BE = 20$ dB (e.g., person blocking effect) and $PL_2(dB) = 68 + 30 \log(d)$, respectively. MIMO channel capacity depends highly on the propagation environment. Specifically, in the LOS channel the received signals experience high correlation which leads to a reduced capacity. Whereas, large number of independent paths exists in NLOS rich-scattering environment, which is close to Rayleigh i.i.d channel thus leads to high capacity. Therefore, the NLOS path loss model $PL_2(dB) = 68 + 30 \log(d)$ is employed in the 60 GHz MIMO system.

Fading margin in the 60 GHz UWB channel is modelled as: $FM[dB] = 4 - 0.5 * B[GHz]$, since previous studies show that FM decreases with channel bandwidth B [P6], and is less than 4 dB for a minimum bandwidth ($B = 500$ MHz) UWB channel with 90% link success probability [P7]. MIMO channel also provides fading improvement relative to a SISO channel. Specifically, fading margin decreases with the number of antenna elements (N) [80][81]. Thus, in the MIMO channel the FM is modeled as: $FM[dB] = 10[dB] - N$, where 10 dB is associated with the FM in traditional 60 GHz SISO channels [P1]. This model limits the MIMO configuration to (10,10), since actually only a small number of MIMO antenna arrays can be constructed in the 60 GHz band [82][83].

As for antenna gains, in MIMO one has to use omnidirectional or low-gain antennas to receive multipaths [84]. Thus, a 10 dB combined gain (the sum of the TX and RX antenna gains) is assumed in the 60 GHz MIMO system. In the 60 GHz UWB channel antenna gains become very important for ensuring that radio links achieve multigigabit capacity of systems. For the convenience of performance and capacity analysis to follow, Table 5-1 provides a summary of the radio link budgets in the 60 GHz UWB and MIMO systems.

5.4 The 60 GHz UWB system performance analysis

Fig. 5-1 shows the combined antenna gains in the 60 GHz UWB channel are shown in when applying the two path loss models and link budget as given in Table 5-1. It should be noted that the path loss model of $LOS + BE$ is more feasible than the NLOS model. Since the *blocking effect* is modeled independently on mobile position, which reflects the real case that movement of persons is quite typical in multipath indoor channels. Whereas, the NLOS model accounts

for high path loss due to large distances generally. In Fig. 5-1 we can see that high-gain antennas are generally required in the 60 GHz UWB channels. The physical problems of high gain antenna systems (easily blocked, poor flexibility and limited mobility) imply that gigabit capacity is difficult to achieve with the 60 GHz UWB system.

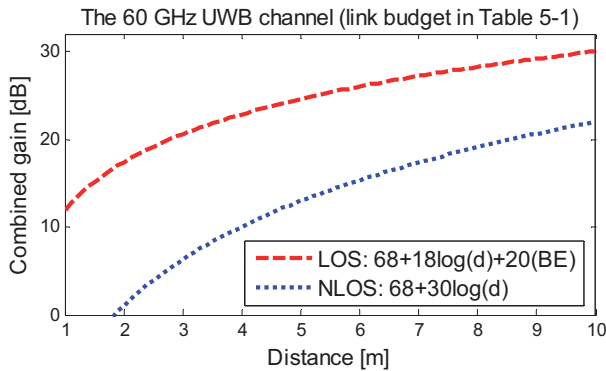


Fig. 5-1. Combined antenna gains in 60 GHz UWB channel with a link budget of Table 5-1.

5.5 The 60 GHz MIMO system capacity analysis

Tests are performed for determining data rate, range and MIMO configuration. Fig. 5-2 shows the test results. It is seen that MIMO configurations of (4,4) and (7,7) can achieve gigabit and multigigabit capacities in 60 GHz MIMO channels. The results of a comparison between the test and experimental channels are shown in Fig. 5-3, which shows the test and experimental MIMO (4,4) channel capacities at different TX-RX separations. It should be noted that parameters used in the test channel of Fig. 5-3 are the same values as in Table 5-1, except that the $P_t = 17$ dBm and $B = 60$ MHz ($N = -90$ dBm) which are the values used in the experimental channel measurements [84]. It is seen that the test results of MIMO (4,4) are in good agreement with the experimental data, which indicates that the parameter values are realistic for the design of radio systems [P8].

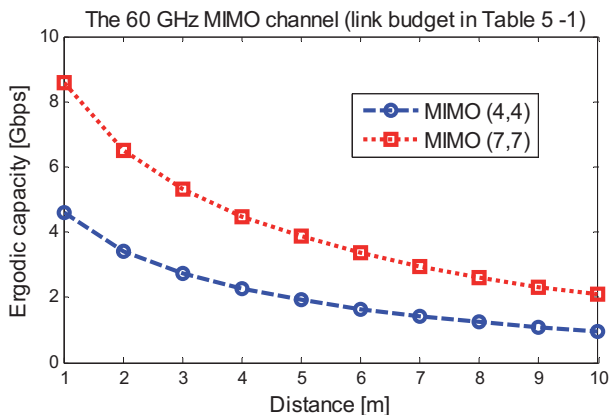


Fig. 5-2. The 60 GHz MIMO configurations of (4,4) and (7,7) can achieve gigabit and multigigabit capacities .

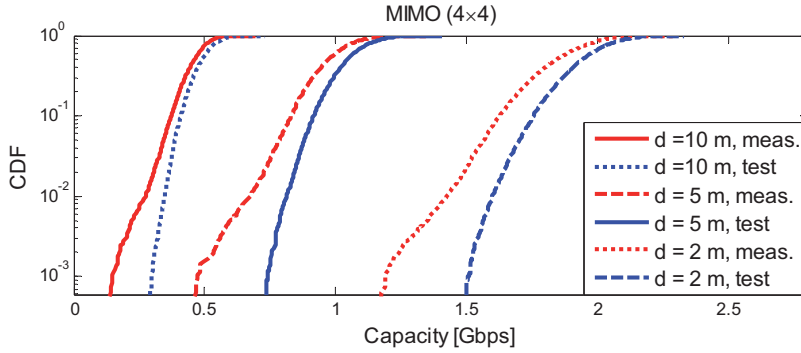


Fig. 5-3. Comparison between the test and experimental MIMO (4,4) channels.

Table 5-1. Link budgets in the 60 GHz UWB and MIMO systems

Frequency	Millimeter-wave 60 GHz	
Rate	> gigabit	
Range	<10 m	
Transmission power	20 dBm	
Implementation loss	6 dB	
Channel parameter	UWB (SNR = 10 dB)	MIMO ($N_T = N_R = N$)
Bandwidth B	2 GHz	100 MHz
Total noise power	-75 dBm	-88 dBm
Fading margin	$FM[dB] = 4 - 0.5 * B[GHz]$	$FM[dB] = 10 - N$ ($2 \leq N \leq 10$)
Path loss model	$PL_1[dB] = 68 + 18 \log(d) + 20(BE)$ $PL_2[dB] = 68 + 30 \log(d)$	$PL_{NLOS}[dB] = 68 + 30 \log(d)$
Combined antenna gain	high gain antennas are required	10 dB is employed
Performance/Capacity	Gigabit communications are quite difficult in the 60 GHz UWB channel.	MIMO (4,4) and (7,7) can achieve gigabit and multigigabit capacities.

6. SUMMARY OF PUBLICATIONS

[P1] Millimeter-wave Propagation Channel Characterization for Short-Range Wireless Communications

This paper presents and analyzes the results of 60 GHz propagation channel measurements performed in various indoor environments for direction-of-arrival and continuous-route measurement campaigns. The statistical parameters and models of the channel such as number of paths, rms delay spread, path loss and shadowing are extracted and derived. Moreover, the interdependencies of different characteristics of the multipath channel are also investigated. A linear relationship between the number of paths and the delay spread is found: negative cross-correlation between the shadow fading and the delay spread can be established: and an upper-bound exponential model of the delay spread and the path loss is developed for estimating the worst case of rms delay spread at given path loss. Based on the direction-of-arrival measurements carried out in a room (LOS) and in a corridor with both LOS and NLOS scenarios, radiowave propagation mechanisms are studied. It is found that considering the direct wave and the first-order reflected waves from smooth surfaces is sufficient in the LOS cases. Transmission loss is very high but diffraction is found to be a significant propagation mechanism in the NLOS propagation environments. The results can be used for the design of 60 GHz radio systems in short-range wireless applications.

[P2] Millimeter-wave Indoor Channel Characterization for Broadband Wireless Local Area Networks

This work is a continuation of [P1]. Specifically, the statistical parameters of the propagation channel like Rice K -factor and cross polarization discrimination (XPD) are investigated. The interdependencies of the Rice K -factor and XPD with channel delay spread are also examined. It is noticed that the K -factor increases with the decrease of channel rms delay spread in general, and a low correlation property between the XPD and delay spread can be established.

[P3] Mm-wave Propagation In Indoor Corridors

In this paper, ray-based models for both LOS and NLOS indoor corridors are presented and compared with experimental results. It is shown that in the LOS corridor signals propagate like in free space and in guided-fashion in near and far zones. A 9-ray model (LOS path plus four first-order and four second-order reflections from the corridor walls, ground and ceiling) is most suitable in characterizing propagation signals in far zone in the environment. In the NLOS corridor, multi-ray models are proposed and a heuristic diffraction coefficient is used in field simulation. Results show that the structure with more rays (eight rays in this work) is adequate in characterizing both average power and variation of signals. The diffracted rays are accurate in characterizing the average decay of signal power. Also, empirical models for NLOS corridors indicate that diffraction is the dominant propagation phenomenon in the environment. Further, multipath power distributions are investigated. It is found that Rayleigh and double-Rayleigh distributions form the bounds for both the LOS and NLOS data. Multiple-Rayleigh distribution can fit the measurement data very accurately.

[4] Multipath Propagation Characterization of Ultra-wide Band Indoor Radio Channels

In this paper, multipath propagation characteristics in UWB (3-10 GHz) indoor channels are investigated. Multipath components are found in single dominant and diffuse paths. Clustering

is a special phenomenon of corridor environment. The UWB channel statistical parameters and models like power delay profiles, rms delay spread, path loss and shadowing are analyzed. Furthermore, the UWB measurement results are compared with the results obtained in traditional wideband 60 GHz indoor channels.

[5] Clustering Characterization for UWB Indoor Communications

In this paper, the cluster characteristics of UWB channels are studied. UWB indoor channels can be generally classified into single- and multi- cluster channels, since a single-exponential decay function and a modified multi-cluster model can be used for characterizing the two cluster channels. The multipath components (MPCs) in the single and multi cluster channels are associated with uniform distribution and limited angular spread, respectively. Moreover, the modified multi-cluster model is compared with the classical Saleh-Valenzuela model. It is shown that the modified cluster model is better in fitting measurement data and that the parameters in the model indicate cluster properties of the propagation channel. The presented results are useful for the design of UWB systems and for standardization groups.

[6] Frequency and Bandwidth Dependency of UWB Propagation Channels

In this paper, the frequency and bandwidth dependencies of propagation in the 3-10 GHz UWB range are investigated by examining the power delay profile, rms delay spread, path loss and shadowing as functions of frequency. Moreover, the multi-band channel characteristics are compared with single-band channels. It is shown that the channel scattering effect depends on the different center frequencies of the multiband channels. Path loss exponent is independent of both frequency and bandwidth, and shadowing STD increases with frequency but decreases with bandwidth of channels.

[7] Experimental Investigation of the Properties of Multiband UWB Propagation Channels

In this paper, the radio link budget in a multiband (dividing the whole frequency range into multiple sub-bands with 500 MHz bandwidth) UWB channel is studied based on empirical analysis of path loss and shadow fading. It is found that the path loss exponent is independent of frequency, and the mean path loss can be modelled as a increasing function of frequency. The standard deviation of shadowing shows a tendency of increasing with frequency. Furthermore, the shadow fading margin with 90% link success probability is found to be fairly low (less than 4 dB) in multiband channels.

[8] Performance and Capacity Analysis of 60 GHz WPAN Channel

In this work, the performance and capacity of both 60 GHz UWB and MIMO channels are analyzed based on experimental channel models and specifications for mm-wave wireless personal area networks (WPANs). In the analysis of the 60 GHz UWB channel, the radio link budget is estimated by applying two experimental channel models where blocking effect is considered and fading margin is modeled as a function of channel bandwidth. Results show that high gain antennas are required in the 60 GHz UWB channel. The physical problems that poor flexibility of high gain antenna systems and easy block effect of the directional signals, indicate that gigabit communications are extremely difficult to achieve in the 60 GHz UWB channel. The 60 GHz MIMO channel capacity is also analyzed. Tests were also performed for determining the gigabit data rate, operation range and configuration in the 60 GHz MIMO channels.

7. CONCLUSIONS

In this thesis, the characteristics of UWB (3-10 GHz) and mm-wave 60 GHz propagation channels are analyzed based on experimental channel measurements, which were performed in various indoor environments for gaining more understanding of channel general properties. Furthermore, the performance and capacities of emerging high throughput radio systems, namely those of 60 GHz UWB and MIMO systems, are analyzed for providing useful information for design of radio systems.

The UWB channel can be generally classified as a single or multiple cluster channel. Specifically, the single-exponential power-decay law and a modified cluster model are proposed for the dual cluster channels. The modified multi-cluster model fits well with the measurement data and with reduced parameters when compared with the Saleh-Valenzuela cluster model. More importantly, the parameters in the proposed multi-cluster model physically denote the clustering properties of channel. Furthermore, frequency and bandwidth dependency of UWB propagation channels are investigated. It is shown that the scattering effect depends on both frequency and structure of the propagation environment. The path loss exponent does not depend on the frequency, but the shadowing standard deviation STD has a clear tendency of increasing with frequency. The bandwidth dependency of the path loss exponent is almost constant, and the shadowing STD decreases with bandwidths. Finally, it is shown that UWB radio is robust to multipath fading.

The mm-wave 60 GHz propagation channel is studied based on the directional-of-arrival and continuous-route measurement campaigns in various indoor environments. The 60 GHz-band propagation mechanisms can be generally concluded as: the first-order reflected waves from smooth surfaces form the main contributions in LOS propagation environments. Diffraction is a significant propagation mechanism in the NLOS cases. Transmission loss through concrete or brick walls is very high, and person blocking effect is about 20 dB in the 60 GHz-band. Ray-based models for LOS and NLOS indoor corridors are proposed. It is found that a 9-ray model (LOS path plus four first-order and four second-order reflections from the corridor walls, ground and ceiling) is the most suitable in characterizing propagation signals in LOS corridor, and the diffracted rays are useful in characterizing the average decay of signal power in NLOS corridors. Moreover, multipath power distributions are investigated. It is shown that Rayleigh and double-Rayleigh distributions form the bounds for both the LOS and NLOS corridor data. The multiple-Rayleigh distribution can fit the measurement data very accurately. Furthermore, interdependencies of channel characteristics such as path loss, shadowing, number of paths, Rice K-factor and cross polarization discrimination with channel delay spread are inspected. Finally, it is pointed out that mm-wave propagation signals are traceable and thus can achieve advantages like robustness to fading.

The performance and capacities of high-rate 60 GHz UWB and MIMO systems are analyzed. Radio link budgets including mean path loss and fading margin for the 60 GHz UWB and MIMO systems are provided. It is shown that high-gain antennas are generally required in 60 GHz UWB system. The physical problems of high gain antenna systems (easily blocked, poor flexibility and limited mobility) indicate that it is difficult to achieve a gigabit capacity using a 60 GHz UWB channel. In the 60 GHz MIMO systems, tests were performed for determining data rate, range and configuration. The test channels are also compared and shown to be in good agreement with the measurement data, thus providing reliable channel parameters in design of 60 GHz MIMO systems.

REFERENCES

- [1] K. Mandke, H. Nam, L. Yerramneni, C. Zuniga, and T. Rappaport, "The evolution of ultra wide band radio for wireless personal area networks," Technology report of *High Frequency Electronics*, 2003 Summit Technical Media, LLC.
- [2] D. Porcine and W. Hirt, "Ultra-wideband radio technology: potential and challenges ahead", *IEEE Commun. Mag.*, pp. 66-74, July 2003.
- [3] R. Fisher, "60 GHz WPAN standardization within IEEE 802.15.3c," *International Symposium on Signals, Systems and Electronics 2007 (ISSSE'07)*, Montreal, Canada, July 30-August 2, 2007, pp. 103-105.
- [4] IEEE 802.15 WPAN Millimeter Wave Alternative PHY Task Group 3c TG3c), www.ieee802.org.
- [5] X. Zhao, S. Geng, L. Vuokko, J. Kivinen, and P. Vainikainen, "Polarization behaviors at 2, 5 and 60 GHz for indoor mobile communications," *Journal of Wireless Personal Communications*, vol. 27, pp. 99-115, July, 2003.
- [6] S. Geng, J. Kivinen, X. Zhao, and P. Vainikainen, "Measurements and analysis of wideband indoor radio channels at 60 GHz," *3rd ESA Workshop on Millimeter Wave Technology and Applications*, Espoo, Finland, May 21-23, 2003, pp. 39-44.
- [7] S. Geng, X. Zhao, J. Kivinen, and P. Vainikainen, "Characterization of multipath dispersion of wideband indoor radio channels at 60 GHz," *IEEE International Symposium on Wireless Personal Multimedia (WPMC04)*, Abano Terme, Italy, Sep. 12-15, 2004, pp. 290-294.
- [8] S. Geng, J. Kivinen, and P. Vainikainen, "Propagation characterization of wideband indoor radio channels at 60 GHz," *IEEE 2005 International Symposium on Microwave, Antenna, Propagation and EMC Technologies for Wireless Communications (MAPE05)*, Beijing, China, Aug. 8-12, 2005, pp. 314-317.
- [9] S. Geng, S. Ranvier, M. Kyrö and P. Vainiainen, "Performance and Capacity Analysis of 60 GHz MIMO Channel for WPANs," *IEEE antenna and Propagat. Soc. International Symposium (AP-S'2009)*, Charleston, USA, June 1-5, 2009, CD-ROM (ISBN 978-1-4244-3647-7), pap321.pdf.
- [10] S. Geng, M. Kyrö, S. Ranvier, K. Haneda and P. Vainiainen, "Feasibility study of emerging high throughput radio systems," *IEEE International workshop on MIMO Channel Measurements and Modeling (IWonCMM09)*, Xian, China, August 25-28, 2009, pap7079.pdf.
- [11] S. Geng, Mikko Kyrö, Veli-Matti Kolmonen, Pertti Vainikainen, "Feasibility study of E-band radio for gigabit point-to-point wireless communications," *Cost 2100 TD(10)10076*, Athens, Greece, Feb. 3-5, 2010.
- [12] A. F. Molisch, "Ultra-wide-band propagation channels," *Proceedings of the IEEE*, vol. 97, pp. 353-371, Feb. 2009.
- [13] T. S. Rappaport, *Wireless Communications*, Prentice Hall PTR, New Jersey, USA, 1996.
- [14] S. K. Yong and C. C. Chong, "An overview of multigigabit wireless through millimeter wave technology: potentials and technical challenges," *EURASIP Journal on Wireless Communications and Networking*, no. 1, pp. 1-10, vol. 2007.
- [15] S. R. Saunders, *Antennas and propagation for wireless communication systems*, John Wiley & Sons, New York, 1999.
- [16] L. Juan-Llacer, L. Ramos, and N. Cardona, "Application of some theoretical models for coverage prediction in macrocell urban environments," *IEEE Trans. Veh. Technol.*, vol. 48, pp. 1463-1468, Sep. 1999.
- [17] V. Erceg, L. J. Greenstein, S. Y. Tjandra, S. R. Parkoff, A. Gupta, B. Kulic, A. A.

- Julius, R. Bianchi, "An empirically based path loss model for wireless channels in suburban environments," *IEEE J. Select. Areas in Commun.*, vol. 17, pp. 1205-1211, July 1999.
- [18] A. Abdi, C. Tepedelenlioglu, M. Kaveh, and G. Giannakis, "On the estimation of the K parameter for Rice fading distribution," *IEEE Commun. Letters*, vol. 5, no. 3, pp. 92-94, Mar. 2001.
- [19] L. J. Greenstein, D. G. Michelson, and V. Erceg, "Moment-method estimation of the Ricean K -factor," *IEEE Commun. Letters*, vol. 3, no. 6, pp. 175-176, June 1999.
- [20] H. Hashemi, "The indoor radio propagation channel," *Proceedings of the IEEE*, vol. 8, pp. 943-968, July 1993.
- [21] M. Nakagami, "The m -distribution-a general formula of intensity distribution of rapid fading," in *Statistical Methods of Radio Wave Propagation*. Pergamon Press, 1960.
- [22] H. Suzuki, "A statistical model for urban radio propagation," *IEEE Trans. Commun.*, vol. 25, pp. 673-680, July 1997.
- [23] V. Erceg, S. J. Fortune, J. Ling, A. J. Rustako, R. A. Valenzuela, "Comparisons of a computer-based propagation prediction tool with experimental data collected in urban microcellular environments," *IEEE J. Select. Areas Commun.*, vol. 15, no. 4, pp. 677-684, May, 1997.
- [24] J. Bach Andersen, "A propagation overview," *Proc. WPMC02, Hawaii*, October, 2002, vol. 1, pp. 1-6.
- [25] X. Zhao and P. Vainikainen, "Multipath propagation study combining terrain diffraction and reflection," *IEEE Transactions on Antennas and Propagation*, vol. 49, no. 8, pp. 1204-1209, Aug. 2001.
- [26] R.M.A. Azzam, "Relationship between the p and s Fresnel reflection coefficients of an interface independent of angle of incidence," *J. Opt. Soc. Am*, A3, pp. 928-929, 1986.
- [27] T. D. Wu, K. S. Chen, J. C. Shi, and A. K. Fung, "A transition model for the reflection coefficient in surface scattering," *IEEE Transactions on Geoscience and Remote Sensing*, vol. 39, pp. 2040-2050, Sep. 2001.
- [28] W. Zhang, J. Lahteenmaki, and P. Vainikainen, "A practical aspect of over-rooftop multiple-building forward diffraction from a low source," *IEEE Transactions on Electromagnetic Compatibility*, vol. 41, pp. 115-119, May 1999.
- [29] H. M. El-Sallabi, I. T. Rekanos, and P. Vainikainen, "A new heuristic diffraction coefficient for dielectric wedges at normal incidence," *IEEE Antennas and Wireless Propagation Letters*, vol. 1, pp. 165-168, 2002.
- [30] G. D. Maliuzhinets, "Excitation, reflection and emission of surface waves from a wedge with given surface impedances," *Sov. Phys. Dokl.*, vol. 3, no. 4, pp. 752-755, 1958.
- [31] Rec. ITU-R, P. 526-7, *Propagation by Diffraction Recommendation*, Geneva, Switzerland, 2001.
- [32] R. J. Luebbers, "Finite conductivity uniform GTD versus knife edge diffraction in prediction of propagation path loss," *IEEE Trans. Antennas Propag.*, vol. 32, no. 1, pp. 70-76, Jan. 1984.
- [33] P. D. Holm, "A new heuristic UTD diffraction coefficient for nonperfectly conducting wedges," *IEEE Trans. Antennas Propag.*, vol. 48, no. 8, pp. 1211-1219, Aug. 2000.
- [34] M. Steinbauer, A. F. Molisch, and E. Bonek, "The double-directional radio channel," *IEEE Antennas Propag. Mag.*, Aug. 2001, vol. 43, no. 4, pp. 51-63.
- [35] D. M. J. Devasirvatham, C. Banerjee, R. R. Murray, D. A. Pappaport, "Four-frequency radiowave propagation measurements of the indoor environment in a large metropolitan commercial building," *Global Telecommunications Conference*, Dec. 1991, vol. 2, pp. 1282 -1286.

- [36] L. Hentila, A. Taparungssanagorn, H. Viittala, and M. Hamalainen, "Measurement and modeling of an UWB channel at hospital," *IEEE International Conference on Ultra-Wideband (ICU05)*, Zurich, Sep. 5-8, 2005, pp. 113-117.
- [37] J. Karedal, S. Wyne, P. Almers, F. Tufvesson, and A. F. Molisch, "A measurement-based statistical model for industrial ultra-wideband channels," *IEEE Transactions on Wireless Communications*, vol. 6, no. 8, pp. 3028-3037, August 2007.
- [38] A. Saleh and R. Valenzuela, "A statistical model for indoor multipath propagation," *IEEE J. Select. Areas Commun.*, vol. 5, no. 2, pp. 128-37, Feb. 1987.
- [39] S. Chang and R. A. Scholtz, "Polarization measurements in a UWB multipath channel," *MILCOM*, 2004, pp. 192-196.
- [40] S. M. Yano, "Investigating the ultra-wideband Indoor wireless channel," *IEEE VTC'2002*, May 6-9, 2002, vol. 3, pp. 1200-1024.
- [41] S. S. Ghassemzadeh, R. Jana, C. W. Rice, W. Turin, V. Tarokh, "A statistical path loss model for in-home UWB channels," in *Proc. of IEEE Conf. Ultra Wideband Systems and Technologies*, Baltimore, USA, May 21-23, 2002, pp. 59-64.
- [42] V. Hovinen, M. Hämäläinen, T. Pätsi, "Ultra wideband Indoor radio channel models: preliminary results," in *Proc. of IEEE Conf. Ultra Wideband Systems and Technologies*, May 21-23, 2002, pp. 75-79.
- [43] J. Kivinen, T. Korhonen, P. Aiko, R. Gruber, P. Vainikainen and S. G. Häggman, "Wideband radio channel measurement system at 2 GHz," *IEEE Transactions Instrumentation and Measurement*, vol. 48, no. 1, pp. 39-44, Feb. 1999.
- [44] J. Kivinen and P. Vainikainen, "Wideband indoor radio channel measurements at 5.3 GHz," in *Proc. of 27th European Microwave Conference Proceedings*, Jerusalem, Israel, Sep. 8-12, 1997, pp. 8-12.
- [45] J. Kivinen, "60-GHz wideband radio channel sounder," *IEEE Transactions Instrumentation and Measurement*, vol. 56, no. 5, pp. 1831-1838, Oct. 2007.
- [46] J. Karedal, S. Wyne, P. Almers, F. Tufvesson, and A. F. Molisch, "UWB channel measurements in an industrial environment," *IEEE GLOBECOM '04*. Vol. 6, Nov. 29-Dec. 3, 2004, pp. 3511 – 3516.
- [47] K. Haneda, J. Takada, and T. Kobayashi, "A parametric uwb propagation channel estimation and its performance validation in an anechoic chamber," *IEEE Trans. Microwave Theory Tech.*, vol. 54, no. 4, pp. 1802-1811, 2006.
- [48] T. Kaiser, F. Zheng, and E. Dimitrov, "An overview of ultra-wide-band systems with MIMO," *Proceedings of the IEEE*, vol. 97, no. 2, pp. 285-312, Feb. 2009.
- [49] A. H. Muqaibel, A. Safaai-Jazi, A.M. Attiya, A. Bayram, S. M. Riad, "Measurement and characterization of indoor ultra-wideband propagation," *IEEE Conf. Ultra Wideband Systems and Technologies*, Reston, USA, May 16-19, 2003, pp. 295-299.
- [50] C. C. Chong, Y. Kim, and S. S. Lee, "Statistical characterization of the UWB propagation channel in various types of high-rise apartments," *IEEE Wireless Communications and Networking Conference (WCNC'05)*, New Orleans, USA, March 2005, vol. 2, pp. 944-949.
- [51] L. J. Greenstein, S. S. Ghassemzadeh, S. C. Hong, and V. Tarokh, "Comparison study of UWB indoor channel models," *IEEE Trans. Wireless Commun.*, vol. 6, no. 1, pp. 128-135, 2007.
- [52] A. Batra, J. Balakrishnan, G. R. Aiello, J. R. Foerster, A. Dabak, "Design of a multiband OFDM system for realistic UWB channel environments," *IEEE Trans. Microwave Theory and Techniques*, vol. 52, no. 9, pp. 2123-2138, Sep. 2004.
- [53] J. Chuang, S. Bashir and D. Michelson, "Automated identification of clusters in UWB channel impulse responses," *Canadian Conference on Electrical and Computer Engineering (CCECE'07)*, April 22-26, 2007, pp. 761-764.

- [54] O. H. Woon and S. Krishnan, "Identification of clusters in UWB channel modeling," *Proc. IEEE Vehicular Technology Conference (VTC'06)*, May 2006, pp. 1-5.
- [55] P. Smulders, "Exploiting the 60 GHz band for local wireless multimedia access: prospects and future directions," *IEEE Communications Magazine*, vol. 40, pp. 140-147, Jan. 2002.
- [56] C. H. Doan, S. Emami, D. A. Sobel, A. M. Niknejad, and R. W. Brodersen, "Design considerations for 60 GHz CMOS radios," *IEEE Communications Magazine*, vol. 12, pp. 132-140, December 2004,
- [57] B. Bosco, R. Emrick, S. Franson, J. Holmes, and S. Rockwell, "Emerging commercial applications using the 60 GHz unlicensed band: opportunities and challenges," *IEEE Wireless and Microwave Technology Conference (WAMICON'06)*, Clearwater Beach, USA, Dec. 4-5, 2006, vol. 1, pp. 1-4.
- [58] C. W. Tolbert and A. W. Straiton, "Attenuation and fluctuation of millimeter radiowaves," *IRE International Convention Record*, vol. 5, March 1957, pp. 12-18.
- [59] A. R. Tharek and J. P. McGeehan, "Propagation and bit error rate measurements within buildings in the millimeter wave band about 60 GHz," *the 8th European Conference on Electronics, (EUROCON'88)*, June 13-17, 1988, pp. 318-321.
- [60] P. F. M. Smulders and A. G. Wagemans, "Biconical horn antennas for near uniform coverage in indoor areas at mm-wave frequencies," *IEEE Transactions on Vehicular Technology*, vol. 43, no. 4, pp. 897-901, Nov. 1994.
- [61] N. Moraitis and P. Constantinou, "Measurements and characterization of wideband indoor radio channel at 60 GHz," *IEEE Transactions on Wireless Communications*, vol. 5, no. 4, pp. 880-889, April 2006.
- [62] A. M. Hammoudeh and G. Allen, "Millimetric wavelengths radiowave propagation for line-of-sight indoor microcellular mobile communications," *IEEE Transactions on Vehicular Technology*, vol. 44, no. 3, pp. 449-460, Aug. 1995.
- [63] Dusan Matic, *OFDM synchronisation and wideband power measurements at 60 GHz for future broadband multimedia communications*, Ph.D. Thesis, Aalborg University, Denmark, 2001.
- [64] M. O. Al-Nuaimi and A. G. Siamarou, "Coherence bandwidth characterization and estimation for indoor Rician multipath wireless channels using measurements at 62.4 GHz," *IEE Proceedings, Microwaves, Antennas and Propagation*, vol. 149, no. 3, pp. 181-187, June 2002.
- [65] Y. Delignon, L. Clavier, V. Lethuc, C. Garnier, and M. Rachdi, "Compound statistical model for 60 GHz channel," *IEEE Vehicular Technology Conference*, Atlantic, USA, Oct. 2001, pp. 1780-1784.
- [66] T. Zwick, T. J. Beukema, and H. Nam, "Wideband channel sounder with measurements and model for the 60 GHz indoor radio channel," *IEEE Transactions on Vehicular Technology*, vol. 54, no. 4, pp. 1266-1277, July 2005.
- [67] H. Yang, M. H. A. J. Herben, and P. F. M. Smulders, "Frequency selectivity of 60-GHz LOS and NLOS indoor radio channels," *the 63rd IEEE Vehicular Technology Conference (VTC'06)*, vol. 6, Melbourne, Australia, May 2006, pp. 2727-2731.
- [68] H. Xu, V. Kukshya, and T. S. Rappaport, "Spatial and temporal characterization of 60 GHz indoor channel," *IEEE Journal on Selected Areas in Communications*, vol. 20, no. 3, pp. 620-630, Apr. 2002.
- [69] C. Demeterscu and C. C. Constantinou, "Scattering by a right-angled lossy dielectric wedge," *Inst. Elect. Eng. Microw. – Antennas Propagat.*, vol. 144, no. 5, pp 392-396, Oct. 1997.
- [70] P. L. Dirmer and S. H. Lin, "Measured frequency diversity improvement for digital radio," *IEEE Transactions on Communications*, vol. 33, no. 1, pp. 106-109, 1985.

- [71] X. Zhao, J. Kivinen, and P. Vainikainen, "Propagation characteristics for wideband outdoor mobile communications at 5.3 GHz," *IEEE J. Select. Areas Communicat.*, vol. 20, no. 3, pp. 507-514, Apr. 2002.
- [72] J. Hansen, "A novel stochastic millimetre-wave indoor radio channel," *IEEE J. Sel. Areas Commun.*, vol. 20, no. 6, pp. 1240-1246, Aug. 2002.
- [73] L. M. Correia, "An overview of wireless broadband communications," *IEEE Commun. Mag.*, vol. 35, no. 1, pp. 28-33, Jan. 1997.
- [74] S. J. MacMullan, and B. D. Patel, "UWB: The solution for wireless A/V cable replacement," *IEEE International Conference on Consumer Electronics*, Las Vegas, USA, Jan. 10-14, 2007, pp. 1-2.
- [75] A. J. Paulraj, D. A. Gore, R. U. Nabar, and H. Bolcskei, "An overview of MIMO communications-a key to Gigabit communications," *Proceedings of the IEEE*, vol. 92, no. 2, pp. 198-218, Feb. 2004.
- [76] P. L. Kafle, A. Intarapanich, A. B. Sesay, J. McRory, and R. J. Davies, "Spatial correlation and capacity measurements for wideband MIMO channels in indoor office environment," *IEEE Transactions on Wireless Communications*, vol. 7, no. 5, pp. 1560-1571, May 2008.
- [77] S. Xi, L. Ren, M. Song and J. Song, "On capacity of MIMO systems in fading channel," *International Conference on Communication Technology (ICCT)*, vol. 2, Beijing, China, April 9-11, 2003, pp.1152-1156.
- [78] I. D. Holland, W. G. Gowley, and C. Burnet, "On the design of gigabit indoor wireless LANs at 60 GHz," <http://epress.lib.uts.edu.au/dspace/bitstream/handle/2100/105/188>
- [79] A. Bourdoux, J. Nsenga, T. V. F. Horlin, L. P. Van, "Air interface and physical layer techniques for 60 GHz WPANs," *IEEE Symposium on Communications and Vehicular Technology*, Liege, Belgium, Nov. 2006, pp. 1-6.
- [80] D. Chizhik, J. Ling, and R. A. Valenzuela, "Wave propagation and slowing the time-fluctuating MIMO channel," *2004 IEEE International Symposium on Antenna and Propagation Society*, vol. 2, June 2004, pp. 1227-1230.
- [81] A. Arvanitis, G. Anagnostou, N. Moraitis, and P. Constantinou, "Capacity study of a multiple element antenna configuration in an indoor wireless channel at 60 GHz," *IEEE 65th Vehicular Technology Conference (VTC2007-Spring)*, Dublin, Ireland, April 22-25, 2007, pp. 609-613.
- [82] J. Y. Park, Y. Wang and T. Itoh, "A 60 GHz integrated antenna array for high-speed digital beamforming applications," *IEEE MTT-S International Microwave Symposium Digest*, vol. 3, Philadelphia, USA, June 2003, pp. 1677-1680.
- [83] K. C. Huang and Z. Wang, "Millimeter-wave circular polarization beam-steering antenna array for gigabit wireless communications," *IEEE Transactions on Antennas and Propagation*, vol. 54, no. 2, pp. 743-746, Feb. 2006.
- [84] S. Ranvier, J. Kivinen, and P. Vainikainen, "Development of a 60 GHz MIMO radio channel measurement system," *IEEE Instrumentation and Measurement Technology*, Ottawa, Canada, May 17-19, 2005, pp. 1878-1882.



ISBN 978-952-60-4318-0 (pdf)
ISBN 978-952-60-4317-3
ISSN-L 1799-4934
ISSN 1799-4942 (pdf)
ISSN 1799-4934

Aalto University
School of Electrical Engineering
Department of Radio Science and Engineering
www.aalto.fi

**BUSINESS +
ECONOMY**

**ART +
DESIGN +
ARCHITECTURE**

**SCIENCE +
TECHNOLOGY**

CROSSOVER

**DOCTORAL
DISSERTATIONS**